Punjab University Journal of Mathematics (2025), 57(12), 1289-1323
https:://doi.org/10.52280/pujm.2025.57(12)02

Mathematical Modeling of Gout Drugs via Neighborhood Eccentricity Descriptors and its Quantitative Structure Property Relationship Analysis

Received
20 August, 2025

Revised
30 March, 2026
21 April, 2026

Accepted
12 May, 2026

Published Online
11 June 2026

*Nadeem Ul Hassan Awan
Department of Mathematics,
Ghazi University D.G Khan,Pakistan

Abdul Ghaffar
Department of Mathematics,
Ghazi University D.G Khan,Pakistan

Abstract. This research article explores the significance of molecular characteristics and structural design of gout drugs. The neighborhood eccentricity topological descriptors obtained from molecular graph theory have been employed on gout drugs. Curvilinear linear regression, random forest and Adaboost regression were used to create quantitative structure property relationship models employing topological indices obtained from these graphs as molecular descriptors. Coefficient of determination, root mean square error, mean absolute error, mean percentage error, and mean absolute percentage error were used to assess model performance. All models endured leave-one-out cross validation to guarantee a detached and trustworthy evaluation. The findings show that random forest and Adaboost are more accurate predictors than linear regression. These results help the development of new gout drugs and demonstrate the efficacy of topological descriptors in conjunction with machine learning for predicting pharmacological attributes. Our findings demonstrate these indices effectively capture and predict important physical characteristics like complexity, polarity, molar refractivity etc. This study explores gout therapeutics such as probenecid, colchicine, allopurinol and fabuxostat etc. Overall, this study supports early stage screening and optimization of gout treatments by offering a reliable, non-experimental and economical method for assessing pharmacological attributes. The study results for Adaboost regression models show exceptional predictive power and assisting in the logical development of gout drugs. The analysis shows a high association between the neighborhood eccentricity descriptors of pharmaceuticals and their physical qualities.

**Corresponding Author*: nadeem.ul.hassan768@gmail.com

AMS (MOS) Subject Classification Codes: 68R10, 05C31, 92C40, 92C99, 90C35

Key Words: M-polynomials, Gout drugs, NEC, QSPR modeling, Random forest, Adaboost, LOOCV.

1. INTRODUCTION

Gout is a metabolic illness that stands as the most rampant type of inflammatory arthritis. One of its distinguishing characteristics is tophus development, which usually results in visible swelling and ongoing pain in the peripheral joints. Fortunately, medical professionals can make an accurate diagnosis with the use of a number of clinical prediction criteria [5]. Crystals of monosodium urate accumulate and deposit in tissues and joints, causing gout. Uric acid crystals can create tophi which are hard, lumpy deposits in the skin[3]. Important clinical questions related to gout were created by a panel of seventy eight international rheumatologists [35]. Gout can cause excruciating, incapacitating arthritis and treatment for flare-ups and continuous urate lowering medicines are part of management [41]. Nephrolithiasis is among the problems that are linked to gout [24]. About 55 million individuals worldwide suffered from gout in 2020. Gout rose with age and was around three times higher in men than in women worldwide. It is expected to affect up to 96 million people by 2050, which could indicate a shift over the next three decades from high-income to low- and middle-income nations [4]. According to data from the global burden of disease survey the United States had the highest point prevalence globally [30]. Additionally, controlling blood pressure, using diuretics sparingly, and maintaining adequate hydration may help avoid flare-ups of gout [10].

Moreover, the applications of graph theory provide a flexible mathematical framework to probe gout drugs characteristics. In the same way a number of physicochemical properties, including surface tension, flashpoint, polar surface area and enthalpy etc. can be predicted using the topological indices. Several topological indices and neighborhood eccentricity descriptors (NEC) of graphs has been the subject of numerous investigations. These indices are computed using graph theoretic mathematical techniques to produce values depicts properties of chemicals [18]. Further, Quantitative structure property relationship (QSPR) is a crucial chemo-informatics technique which allows scientists to prognostication the biological activity or characteristics of drugs by examining their molecular structures. This method establishes relationships between chemical structure and activity using statistical methods which makes it easier to implement [25,29]. Chemistry and pharmacology have made extensive use of these descriptors, which are produced utilizing the molecular structure [33]. Degree, distance, eigenvalue, entropy, temperature etc. descriptors are some of the different forms of Tds. With the assistance of graph theory chemists can better comprehend chemical processes and design new medications and materials by gaining insights into molecular behavior[15]. The study of Tds resulted in the creation of more than three thousand indices that represent the structural characteristics of graphs. Using multiple linear regressions, Tamilarasi et al. [37] created four new indicators. In their recent QSPR research of COVID-19 medications employing TIs, Suresh et al. employed

multiple linear regressions Instead of using simple graphs; they took into consideration the multi-graph of drugs [36]. Using QSAR modeling, Rasheed et al. examined new indices and thermodynamic characteristics of eye infection treatments [32,34,38].

Second, this study is the first to use molecular NEC topological descriptors in conjunction with random forest (RF) and Adaboost regression to predict physicochemical characteristics related to glaucoma treatments. Third, to systematically evaluate the performance of traditional versus contemporary machine learning models, a unified comparative modeling framework utilizing curvilinear regression, random forest regression (RF), and Adaboost was developed. Further, leave-one-out cross-validation (LOOCV), a suitable validation technique for small datasets, was used to completely assess the model's resilience and prediction reliability. This work offers a novel, repeatable modeling approach for gout medicines and gives important direction for future rational drug design and optimization efforts by combining chemical graph theory, machine learning techniques, and rigorous statistical validation. Figure 1 shows the chemical structures of the medications that were assessed.

Further, this study concentrates on gout drugs and offering insights in order to predict drug characteristics so as to efficiently predict these physical properties. QSPR models generate prediction models from datasets for corresponding physicochemical properties using a variety of computational techniques like curvilinear regression analysis [11,16]. The QSPR analysis decrease the time and expenses related to experimental testing in drugs discovery. Chemists use techniques such as QSPR, QSTR, and QSAR analysis to generate new medications based on information about the physicochemical features of the molecules. The investigation on the first Zagreb index, hyper Zagreb index[13], atom-bond connectivity index [6], Randic index [31], sum connectivity index [45], geometric-arithmetic index [21], Sombor index [14], and Nirmala index [23] second Zagreb index [28], harmonic index [7]. Kirmani et al. Covid-19 drugs are studies with Tds for exploring the QSPR of analysis [20]. Gnanaraj et al. used the QSPR model to investigate the properties of NASID pharmaceuticals [12]. QSPR modeling technique has versatile predictive ability in discovery of drugs. This was efficiently applied by Zhou et al. [46] and thermodynamic features are found correctly. Zaman et al. found some model of novel drugs applied in blood cancer treatment [42]. Nasir modeling in colorectal disease demonstrates that the QSPR technique is the most effective in predicting the properties of medications [27] and also yields valuable results about blood cancer [26]. Researchers were inspired to use QSPR approaches by Zang et al. flexible analysis of medications for schizophrenia [44]. Kulli Nirmala indices have influential envisaging supremacy [22]. Researchers Koam et al. looked at the entropy of nanotubes in 2023 [21]. Plentiful investigation on Tds is done by Imran et al. and is famous in investigating topological indices of dendrimers [16].

Diverse drugs graph theoretical results are mentioned by Wei et al. [39]. Fractional and fractal-fractional models are for studying intricate biological and epidemiological systems, such as COVID-19 dynamics and virus transmission in honeybees [8]. Additionally; they emphasize how memory effects and fractional operators can be used to predict environmental issues like sustainability and carbon dioxide emissions[9]. Rigid frameworks for managing uncertainty in fractional differential equations are provided by theoretical advancements like the extension of some inequality [19]. To better understand system behavior and increase prediction accuracy, sophisticated mathematical methods like stability

theory and numerical simulations are frequently employed [1]. Fractional order modeling in practical applications by providing enhanced analysis, control methods and long term insights [17] and these studies efficiently highlight it. Comparative analysis of Coid-19 drugs via NEC is investigated [18] and motivated us to probe into gout drugs and best models are found with these descriptors. This study has focused on gout drugs with Pubchem CID are colchicine, lesinurad allopurinol, februxostat, prednisone, oxypurinol, probenecid, methotrexate, topiroxostat, arhalofenate and verinurad. To ascertain the NEC, we created visual representations of the drug structures in Fig 2. Lesinurad is a uric acid transporter inhibitor that is used to treat hyperuricemia linked to gout in patients whose xanthine oxidase inhibitor monotherapy is insufficient to regulate their uric acid levels. Allopurinol and fabuxostat are used to treat chronic hyperuricemia. Prednisone is a corticosteroid that is used to treat. Tophaceous gout and hyperuricemia are all treated with the drug probenecid. Methotrexate is an anti-cancer medication used to treat severe gout, juvenile rheumatoid arthritis, and a wide range of malignancies. Topiroxostat and its metabolites have been demonstrated to be immune to renal problems. Verinurad has been investigated in the basic research and treatment of gout and asymptomatic hyperuricemia.

First of all we employed NEC based edge partition technique on gout drugs. Then expedite the calculations and data processing by implementing python and machine learning techniques like random forest and Adaboost. Additionally on applying python, we used various higher order regression models and looked into the QSPR analysis of the computed neighborhood eccentricity descriptors, as shown in Table 2 to Table 7. Section 4 defines the NEC-polynomials of drugs in Table 1 whereas the article's subsection 4.2 discusses regression models and errors. The authors implemented following software: Microsoft Excel, python, and SPSS to expedite the computation process.
Aims and objectives of this work include the following: The main goal of this research is to create reliable QSPR models by combining cutting-edge machine learning methods, particularly Random Forest and Adaboost, with neighborhood-based topological indices. The goal of the study is to better understand how neighborhood descriptors may predict structural information and assess how well they can represent the physicochemical properties of chemical molecules.

i. This study introduces the use of neighborhood eccentricity topological descriptors as informative molecular descriptors within ensemble machine learning frameworks, which has not been extensively explored in existing QSPR literature.

ii. Gout drugs molecular graphs are successfully analyzed by computing different neighborhood eccentricity topological descriptors (NEC) QSPR analysis.

iii. Curvilinear linear regressions are used to evaluate the association between seven important physicochemical parameters and eight topological descriptors.

iv. Researchers commonly employ linear regression models. However, this study differs by applying curvilinear regression models (degree: 1, 2, 3, and 6) to gout medications along with random forest and Adaboost.

v. QSPR models are built using topological descriptors that exhibit a strong association with these characteristics.

vi. We also compare the actual and anticipated values obtained from regression models.

2. MATERIAL AND METHODS

2.1. **NEIGHBORHOOD ECCENTRICITY INDICES MESUREMENT.** In this part of study, $G = (V, E)$ represents the molecular structure of a chemical compound, $V(G)$ is vertex set and $E(G)$ is edges set (bonds). The length of the shortest path is denoted $d(u, v)$ and called distance between vertices. For two connected vertices i.e. $d(u, v) = 1$. The eccentricity of vertex is $\varepsilon_u = \max\{d(u, v) \mid u \in V(G)\}$, the EC–polynomial in a graph G is defined as:
$EC(G, r, y) = \sum_{i \leq j} \mu_{ij} x^i y^j$ where $\mu_{ij} = |\varepsilon_{ij}|$ and $\varepsilon_{ij} = \{uv \in E(G) \mid \varepsilon_u = i, \varepsilon_v = j\}$
The neighborhood eccentricity of a vertex u in a graph G is defined as the sum of eccentricity of the vertices adjacent to u in G and denoted by (u). The NEC-polynomial [42] based on the neighborhood eccentricity of vertices in a graph G which is introduced as follows: $NEC(G, r, y) = \sum_{i \leq j} n_{ij} x^i y^j$ where $n_{ij} = |E_{ij}|$ and $E_{ij} = \{uv \in E(G) \mid \tau_u = i, \tau_v = j\}$
The following calculation with this operation utilized in this article and mentioned under:

$$D_x = x\frac{\partial h(x,y)}{\partial x}, D_y = y\frac{\partial h(x,y)}{\partial y}, \quad S_x = \int_0^x \frac{h(t,y)}{t}\, dt, \quad S_y = \int_0^y \frac{h(x,t)}{t}\, dt,$$

$$\psi_k(h(x,y)) = x^k h(r,y), J(h(x,y)) = h(y,y)$$

Gout drugs properties with units include enthalpy of vaporization (E, kJ/mol), complexity (C), momolar volume (MV, cm^3), polarity (P, cm^3) and molecular weight (MW, g/mol). In QSPR modeling, physicochemical characteristics are important for drug design, metabolism, absorption, distribution, and toxicity assessment. The current research with NEC-polynomials applications and curvilinear regression models in the development and application of topological descriptors is an important factor in the advancement of computational chemistry and molecular modeling of drugs [18]. We simply write $NEC(G, x, y) = N$ in the Table 1.

2.2. **CURVILINEAR REGRESSION MODELS FOR GOUT DISEASE DRUGS.** In this part of investigation, we utilized linear, quadratic, cubic and bicubic regression models on physical properties and topological descriptors. The model was evaluated using the correlation coefficient (R). For instance, the RMSE number will be zero if the correlation coefficient is one and all of the points lie on the regression line, and are significant [2, 43]. The ideal model was determined by utilizing the highest R^2, R, F and least standard error (SE) values. The linear QSPR model describes that is straight line. The following equation represents linear regression:

$$P = a + k_1 T_1. \tag{1}$$

where the error term k_1 is the slope coefficient, and a is the y-intercept. The quadratic QSPR model represents a parabolic relationship, which is represented as a U-shaped curve.

$$P = a + k_1 T_1 + k_2 T_1^2. \tag{2}$$

The T_1^2 term makes the model applicable to data that changes direction just once by enabling it to capture parabolic patterns. In order to represent more intricate curves, the cubic

regression model adds a third-degree polynomial term.

$$P = a + k_1 T_1 + k_2 T_1^2 + k_3 T_1^3. \quad (3)$$

This can depict S-shaped curves with two points of inflection, offering flexibility in fitting data with fluctuating rates of rise and fall. An explanation of the Bicubic QSPR Model For two independent variables, the cubic regression is extended. It extends polynomial regression to two independent variables. It is expressed as follows:

$$P = a + K_1 T_1 + K_2 T_1^2 + K_3 T_1^3 + K_4 T_1^4 + K_5 T_1^5 + K_6 T_1^6. \quad (4)$$

Here topological descriptor is T_1. All of the above equations 1- 4 represent the regression model equations that will utilized to access QSPR modeling of gout drugs. Standard statistical criteria were used to assess the interpretability and reliability of the models. Random forest (RF), which enables nonlinear modeling through kernel functions while effectively controlling model complexity. Additionally, Adaboost, a gradient boosting ensemble learning algorithm, was used to model complex nonlinear relationships and higher order interactions among the descriptors. A LOOCV cross-validation was used to guarantee reliable and objective model evaluation across all methods due to the dataset's very short size. In order to ensure that each compound contributed once to model validation, each compound was iteratively held out as the test sample while the remaining compounds were used for model training. Throughout the analysis, a fixed random seed (seed 42) was used to ensure reproducibility of the results. Standard feature scaling was used to normalize all input descriptors before model fitting. A grid-search process included within the LOOCV framework was used to optimize the hyper parameter for the random forest and Adaboost models. The reported metrics are the mean values averaged throughout all LOOCV iterations, and model performance was assessed consistently across all modeling methodologies.

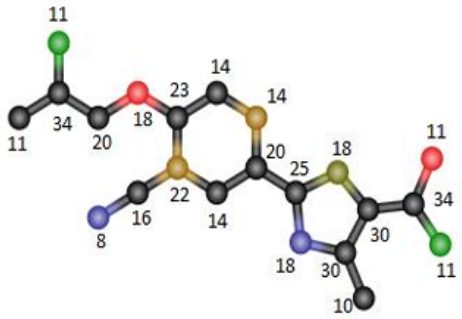

FIGURE 1. Neighborhood eccentricity based partitioning of fabuxostat vertices.

3. RESULTS AND DISCUSSION

In this section, we will thoroughly compute the neighborhood eccentricity descriptors for gout drugs.

TABLE 1. Formulae to compute the neighborhood eccentricity descriptors.

Topological descriptors	Mathematical expression	Derivation from
NE_1	$\sum_{xy\in E}(\mu(x)+\mu(y))$	$(D_x+D_y)P(x,y)(1,1)$
NE_2	$\sum_{xy\in E}\mu(x)\mu(y)$	$(D_xD_y)P(x,y)(1,1)$
NFE	$\sum_{xy\in E}\mu(x)^2+\mu(y)^2$	$(D_x^2+D_y^2)P(x,y)(1,1)$
NRE	$\sum_{xy\in E}(\mu(x)\mu(y))(\mu(x)+\mu(y))$	$(D_xD_y)(D_x+D_y)P(x,y)(1,1)$
$NSDE$	$\sum_{xy\in E}\frac{\mu(y)}{\mu(x)}+\frac{\mu(x)}{\mu(y)}$	$(D_xS_y+S_yD_x)P(x,y)(1,1)$
$NISIE$	$\sum_{rx\in E}\frac{\mu(x)\mu(y)}{\mu(y)+\mu(x)}$	$(S_xJD_yD_x)P(x,y)(1,1)$
NHE	$\sum_{xy\in E}\frac{2}{\mu(x)+\mu(y)}$	$(2S_x)P(x,y)(1,1)$
NAE	$\sum_{xy\in E}\left[\frac{\mu(x)\mu(y)}{\mu(x)+\mu(y)-2}\right]^3$	$(S_y^2\psi_2JD_y^3D_x^3)P(x,y)(1,1)$

3.1. **COMPUTATION OF NEIGHBORHOOD ECCENTRICITY INDICES.** This part of investigation is dedicated to NEC-polynomials of fabuxostat with detail calculation.

Theorem 1. Let A_1 be fabuxostate graph. Then its neighborhood eccentricity polynomial is given as:

$$NEC(A_1,x,y)=x^{30}y^{34}+x^{30}y^{30}+x^{22}y^{23}+x^{20}y^{34}+x^{20}y^{25}+2x^{18}y^{30}+2x^{18}y^{25}+x^{18}y^{23}+x^{18}y^{20}+x^{16}y^{22}+x^{14}y^{23}+x^{14}y^{22}+2x^{14}y^{20}+x^{14}y^{14}+4x^{11}y^{34}+x^{10}y^{30}+x^{8}y^{16}.$$

Proof: Fabuxostate has |V|=22 and |E|= 23 and edge partition for it is mentioned as:
$|E_{30,34}|=1, |E_{30,30}|=1, |E_{22,23}|=1, |E_{20,34}|=1, |E_{20,25}|=1, |E_{18,30}|=2, |E_{18,25}|=2, |E_{18,23}|=1,$
$|E_{18,20}|=1, |E_{16,22}|=1, |E_{14,23}|=1, |E_{14,22}|=1, |E_{14,20}|=2, |E_{14,14}|=1, |E_{14,34}|=1, |E_{11,34}|=4,$
$|E_{18,16}|=1$. Then, we have:

$$NEC(A_1,x,y)=x^{30}y^{34}+x^{30}y^{30}+x^{22}y^{23}+x^{20}y^{34}+x^{20}y^{25}+2x^{18}y^{30}+2x^{18}y^{25}+x^{18}y^{23}+x^{18}y^{20}+x^{16}y^{22}+x^{14}y^{23}+x^{14}y^{22}+2x^{14}y^{20}+x^{14}y^{14}+4x^{11}y^{34}+x^{10}y^{30}+x^{8}y^{16}.$$

Theorem 2 Let A_1 be fabuxostate graph. Taking Figure 1, various neighborhood eccentricity descriptors for the graph are calculated as:

i. $NE_1(A_1)$= 980 v. $NSDE(A_1)=55.4884$
ii. $NE_2(A_1)=10022$ vi. $NISIE(A_1)=224.957$
iii. $NFE(A_1)=23530$ vii. $NHE(A_1)=1.3071$
iv. $NRE(A_1)=465762$ viii. $NAE(A_1)=29249$

Proof:

$$NE_1(A_1)=(D_x+D_y)P(x,y)(1,1)$$

$$=64x^{30}y^{34}+60x^{30}y^{30}+45x^{22}y^{23}+54x^{20}y^{34}+45x^{20}y^{25}+96x^{18}y^{30}$$

$$+86x^{18}y^{25}+41x^{18}y^{23}+38x^{18}y^{20}+38x^{16}y^{22}+37x^{14}y^{23}+36x^{14}y^{22}$$
$$+68x^{14}y^{20}+28x^{14}y^{14}+180x^{11}y^{34}+40x^{10}y^{30}+24x^{8}y^{16}=980.$$

$$NE_2(A_1)=(D_xD_y)P(x,y)(1,1)$$

$$=1020x^{30}y^{34}+900x^{30}y^{30}+506x^{22}y^{23}+680x^{20}y^{34}+500x^{20}y^{25}$$

$$+1080x^{18}y^{30}+900x^{18}y^{25}+414x^{18}y^{23}+360x^{18}y^{20}+352x^{16}y^{22}$$

$$+322x^{14}y^{23}+308x^{14}y^{22}+560x^{14}y^{20}+196x^{14}y^{14}+1496x^{11}y^{34}$$
$$+300x^{10}y^{30}+128x^{8}y^{16}=10022.$$

$$NFE(A_1)=(D_x^2+D_y^2)P(x,y)(1,1)$$

$$=2056x^{30}y^{34}+1800x^{30}y^{30}+1013x^{22}y^{23}+1556x^{20}y^{34}+1025x^{20}y^{25}$$

$$+2448x^{18}y^{30}+1898x^{18}y^{25}+853x^{18}y^{23}+724x^{18}y^{20}+740x^{16}y^{22}$$

$$+725x^{14}y^{23}+680x^{14}y^{22}+1192x^{14}y^{20}+392x^{14}y^{14}+5108x^{11}y^{34}$$

$+1000x^{10}y^{30} + 320x^{8}y^{16} = 23530.$

$$NRE\,(A_1) = (D_xD_y)(D_x + D_y)P(x,y)(1,1)$$

$$= 65280x^{30}y^{34} + 54000x^{30}y^{30} + 22770x^{22}y^{23} + 36720x^{20}y^{34}$$

$$+22500x^{20}y^{25} + 51840x^{18}y^{30} + 38700x^{18}y^{25} + 16974x^{18}y^{23}$$

$$+13680x^{18}y^{20} + 13376x^{16}y^{22} + 11914x^{14}y^{23} + 11088x^{14}y^{22}$$

$$+19040x^{14}y^{20} + 5488x^{14}y^{14} + 67320x^{11}y^{34} + 12000x^{10}y^{30}$$

$+3072x^{8}y^{16}$=465762.

$$NSDE\,(A_1) = (D_xS_y + S_yD_x)P(x,y)(1,1)$$

$$= \frac{514x^{30}y^{34}}{255} + 2x^{30}y^{30} + \frac{1013x^{22}y^{23}}{506} + \frac{389x^{20}y^{34}}{170} + \frac{41x^{20}y^{25}}{20}$$

$$+\frac{68x^{18}y^{30}}{15} + \frac{949x^{18}y^{25}}{225} + \frac{853x^{18}y^{23}}{414} + \frac{181x^{18}y^{20}}{90} + \frac{185x^{16}y^{22}}{88}$$

$$+\frac{725x^{14}y^{23}}{322} + \frac{170x^{14}y^{22}}{77} + \frac{149x^{14}y^{20}}{35} + 2x^{14}y^{14} + \frac{2554x^{11}y^{34}}{187}$$

$+\frac{10x^{10}y^{30}}{3} + \frac{5x^{8}y^{16}}{2}$ = 55.4884.

$$NISIE\,(A_1) = (S_xJD_xD_y)P(x,y)(1,1)$$

$$= \frac{255x^{64}}{16} + 15x^{60} + \frac{340x^{54}}{27} + \frac{45x^{48}}{2} + \frac{278x^{45}}{5} + \frac{900x^{43}}{43} + \frac{414x^{41}}{41}$$

$$+\frac{15x^{40}}{2} + \frac{356x^{38}}{19} + \frac{322x^{37}}{37} + \frac{77x^{36}}{9} + \frac{280x^{34}}{17} + 7x^{28} + \frac{16x^{24}}{3}$$

$$NHE\,(A_1) = (2S_xJ)P(x,y)(1,1)$$

$$= \frac{x^{64}}{32} + \frac{x^{60}}{30} + \frac{x^{54}}{27} + \frac{x^{48}}{12} + \frac{4x^{45}}{15} + \frac{4x^{43}}{43} + \frac{2x^{41}}{41} + \frac{x^{40}}{20} + \frac{2x^{38}}{19} + \frac{2x^{37}}{37}$$

$+\frac{x^{36}}{18} + \frac{2x^{34}}{17} + \frac{x^{28}}{14} + \frac{x^{24}}{12}$ = 1.3071.

$$NAE\,(A_1) = (S_y^2\psi_{-2}JD_x^3D_y^3)P(x,y)(1,1)$$

$$= \frac{132651000x^{62}}{29791} + \frac{91125000x^{58}}{24389} + \frac{4913000x^{52}}{2197} + \frac{39366000x^{46}}{12167}$$

$$+\frac{463808712x^{43}}{79507} + \frac{182250000x^{41}}{68921} + \frac{2628072x^{39}}{2197} + \frac{3375000x^{38}}{6859}$$

$$+\frac{1410472x^{36}}{729} + \frac{97336x^{35}}{125} + \frac{3652264x^{34}}{4913} + \frac{42875x^{32}}{32} + \frac{941192x^{26}}{2197}$$

$+\frac{262144x^{22}}{1331} = 29249.$

Theorem 3. Let A_2 be colchicine graph. Then its neighborhood eccentricity polynomial is given as:

$$\begin{aligned} NEC(A_2,x,y) &= x^{27}y^{27}+x^{25}y^{26}+x^{22}y^{25}+x^{21}y^{22}+x^{20}y^{27}+x^{20}y^{26}+2x^{20}y^{22}+x^{20}y^{21}+ \\ &\quad x^{20}y^{20}+x^{18}y^{25}+x^{16}y^{28}+2x^{16}y^{27}+x^{16}y^{26}+3x^{16}y^{22}+x^{16}y^{21}+x^{15}y^{22}+ \\ &\quad x^{14}y^{22}+x^{14}y^{20}+x^{14}y^{16}+x^{14}y^{15}+2x^{10}y^{20}+2x^{9}y^{28}+x^{9}y^{27}+x^{9}y^{18}+x^{8}y^{16}. \end{aligned}$$

Proof: Colchicine has |V|=29 and |E|= 31 and edge partition for it is mentioned as:
$|E_{27,27}|=1, |E_{25,26}|=1, |E_{22,25}|=1, |E_{21,22}|=1, |E_{20,27}|=1, |E_{20,26}|=1, |E_{20,22}|=2, |E_{20,21}|=1,$
$|E_{20,20}|=1, |E_{18,25}|=1, |E_{16,28}|=1, |E_{16,27}|=2, |E_{16,26}|=1, |E_{16,22}|=3, |E_{16,21}|=1, |E_{15,22}|=1,$
$|E_{14,22}|=1, |E_{14,20}|=1, |E_{14,16}|=1, |E_{14,15}|=1, |E_{10,20}|=2, |E_{9,28}|=2, |E_{9,27}|=1, |E_{9,18}|=1,$
$|E_{8,16}|=1$. Then, we have:

$$\begin{aligned} NEC(A_2,x,y) &= x^{27}y^{27}+x^{25}y^{26}+x^{22}y^{25}+x^{21}y^{22}+x^{20}y^{27}+x^{20}y^{26}+2x^{20}y^{22}+x^{20}y^{21}+ \\ &\quad x^{20}y^{20}+x^{18}y^{25}+x^{16}y^{28}+2x^{16}y^{27}+x^{16}y^{26}+3x^{16}y^{22}+x^{16}y^{21}+x^{15}y^{22}+ \\ &\quad x^{14}y^{22}+x^{14}y^{20}+x^{14}y^{16}+x^{14}y^{15}+2x^{10}y^{20}+2x^{9}y^{28}+x^{9}y^{27}+x^{9}y^{18}+x^{8}y^{16}. \end{aligned}$$

Theorem 4 Let A_2 be colchicine graph. Taking Figure 2, various neighborhood eccentricity descriptors for the graph are calculated as:

i. $NE_1(A_2)$ =1206 v. $NSDE(A_2)$ =70.519
ii. $NE_2(A_2)$ =11510 vi. $NISIE(A_2)$ = 285.653
iii. $NFE(A_{2\ 1})$ =25338 vii. $NHE(A_2)$ =1.648
iv. $NRE(A_2)$ =476428 viii. $NAE(A_2)$ = 32034.961

Theorem 5. Let A_3 be lesinurad graph. Then its neighborhood eccentricity polynomial is given as:

$$\begin{aligned} NEC(A_3,x,y) &= x^{26}y^{31}+x^{25}y^{26}+x^{22}y^{25}+2x^{21}y^{31}+x^{21}y^{21}+3x^{20}y^{22}+ \\ &\quad x^{20}y^{20}+x^{18}y^{31}+x^{18}y^{25}+2x^{18}y^{18}+x^{16}y^{26}+2x^{16}y^{22}+ \\ &\quad 2x^{16}y^{18}+2x^{15}y^{22}+x^{15}y^{15}+x^{14}y^{20}+x^{14}y^{16}+2x^{10}y^{31}+x^{7}y^{22}. \end{aligned}$$

Proof: Lesinurad has |V|=24 and |E|= 27 and edge partition for it is mentioned as:
$|E_{26,31}|=1, |E_{25,26}|=1, |E_{22,25}|=1, |E_{21,31}|=2, |E_{21,21}|=1, |E_{20,22}|=3, |E_{20,20}|=1, |E_{18,31}|=1,$
$|E_{18,25}|=1, |E_{18,18}|=2, |E_{16,26}|=1, |E_{16,22}|=2, |E_{16,18}|=2, |E_{15,22}|=2, |E_{15,15}|=1, |E_{14,20}|=1,$
$|E_{14,16}|=1, |E_{10,31}|=2, |E_{7,22}|=1$.Then, we have:

$$\begin{aligned} NEC(A_3,x,y) &= x^{26}y^{31}+x^{25}y^{26}+x^{22}y^{25}+2x^{21}y^{31}+x^{21}y^{21}+3x^{20}y^{22}+ \\ &\quad x^{20}y^{20}+x^{18}y^{31}+x^{18}y^{25}+2x^{18}y^{18}+x^{16}y^{26}+2x^{16}y^{22}+ \\ &\quad 2x^{16}y^{18}+2x^{15}y^{22}+x^{15}y^{15}+x^{14}y^{20}+x^{14}y^{16}+2x^{10}y^{31}+x^{7}y^{22}. \end{aligned}$$

Theorem 6 Let A_3 be lesinurad graph. Taking Figure 2, various neighborhood eccentricity descriptors for the graph are calculated as:

i. $NE_1(A_3) = 1096$ v. $NSDE(A_3) = 60.017$
ii. $NE_2(A_3) = 11510$ vi. $NISIE(A_3) = 262.252$
iii. $NFE(A_3) = 23858$ vii. $NHE(A_3) = 1.370$
iv. $NRE(A_3) = 473732$ viii. $NAE(A_3) = 31966.926$

Theorem 7. Let A_4 be allopurinol graph. Then its neighborhood eccentricity polynomial is given as:

$$NEC(A_4,x,y) = 2x^{10}y^{11}+3x^{7}y^{11}+x^{7}y^{10}+4x^{7}y^{8}+x^{3}y^{11}.$$

Proof: Allopurinol has |V|=10 and |E|= 11 and edge partition for it is mentioned as:
$|E_{10,11}|=2, |E_{7,11}|=3, |E_{7,10}|=1, |E_{7,8}|=4, |E_{3,11}|=1$. Then, we have:

$$NEC(A_4,x,y) = 2x^{10}y^{11}+3x^{7}y^{11}+x^{7}y^{10}+4x^{7}y^{8}+x^{3}y^{11}.$$

Theorem 8. Let A_4 be allopurinol graph. Taking Figure 2, various neighborhood eccentricity descriptors for the graph are calculated as:

i. $NE_1(A_4) = 187$ v. $NSDE(A_4) = 24.781$
ii. $NE_2(A_4)$ =778 vi. $NISIE(A_4) = 44.718$
iii. $NFE(A_4) = 1683$ vii. $NHE(A_4) = 1.318$
iv. $NRE(A_4) = 13790$ viii. $NAE(A_4) = 1164.642$

Theorem 9. Let A_5 be probenecid graph. Then its neighborhood eccentricity polynomial is given as:

$$\begin{aligned} NEC(A_5,x,y) &= x^{32}y^{37}+x^{31}y^{37}+x^{26}y^{34}+x^{22}y^{32}+x^{22}y^{31}+x^{21}y^{22}+ \\ &\quad x^{20}y^{34}+2x^{20}y^{32}+x^{20}y^{26}+2x^{20}y^{21}+x^{18}y^{34}+x^{18}y^{20}+ \\ &\quad x^{17}y^{37}+x^{16}y^{26}+x^{16}y^{22}+x^{16}y^{17}+x^{14}y^{32}+2x^{14}y^{21}+ \\ &\quad x^{14}y^{16}+x^{11}y^{32}+x^{11}y^{22}+x^{10}y^{31}+x^{9}y^{37}+x^{8}y^{34}+x^{8}y^{32}+x^{6}y^{21}. \end{aligned}$$

Proof: Probenecid has |V|=26 and |E|= 29and edge partition for it is mentioned as:
$|E_{32,37}|=1, |E_{31,37}|=1, |E_{26,34}|=1, |E_{22,32}|=1, |E_{22,31}|=1, |E_{21,22}|=1, |E_{20,34}|=1, |E_{20,32}|=2,$

$|E_{20,26}|=1, |E_{20,21}|=2, |E_{18,34}|=1, |E_{18,20}|=1, |E_{17,37}|=1, |E_{16,26}|=1, |E_{16,22}|=1, |E_{16,17}|=1,$
$|E_{14,32}|=1, |E_{14,21}|=2, |E_{14,16}|=1, |E_{11,32}|=1, |E_{11,22}|=1, |E_{10,31}|=1, |E_{9,37}|=1, |E_{8,34}|=1,$
$|E_{8,32}|=1, |E_{6,21}|=1$. Then, we have:

$$NEC(A_5, x, y) = x^{32}y^{37} + x^{31}y^{37} + x^{26}y^{34} + x^{22}y^{32} + x^{22}y^{31} + x^{21}y^{22} + x^{20}y^{34} + 2x^{20}y^{32} + x^{20}y^{26} + 2x^{20}y^{21} + x^{18}y^{34} + x^{18}y^{20} + x^{17}y^{37} + x^{16}y^{26} + x^{16}y^{22} + x^{16}y^{17} + x^{14}y^{32} + 2x^{14}y^{21} + x^{14}y^{16} + x^{11}y^{32} + x^{11}y^{22} + x^{10}y^{31} + x^{9}y^{37} + x^{8}y^{34} + x^{8}y^{32} + x^{6}y^{21}.$$

Theorem 10 Let A_5 be probenecid graph. Taking Figure 2, various neighborhood eccentricity descriptors for the graph are calculated as:

i. $NE_1(A_5) = 1308$ v. $NSDE(A_5) = 73.737$
ii. $NE_2(A_5) = 14175$ vi. $NISIE(A_5) = 296.579$
iii. $NFE(A_5) = 33666$ vii. $NHE(A_5) = 1.353$
iv. $NRE(A_5) = 711818$ viii. $NAE(A_5) = 44303.755$

Theorem 11. Let A_6 be a oxypurinol graph. Then its neighborhood eccentricity polynomial is given as:

$$NEC(A_6, x, y) = 2x^{11}y^{12} + x^9y^{11} + x^9y^9 + x^8y^{12} + x^8y^9 + 2x^7y^{13} + 2x^7y^{12} + x^4y^{13} + x^3y^{12}.$$

Proof: Oxypurinol has |V|=11 and |E|= 12 and edge partition for it is mentioned as:
$|E_{11,12}|=2, |E_{9,11}|=1, |E_{9,9}|=1, |E_{8,12}|=1, |E_{8,9}|=1, |E_{7,13}|=2, |E_{7,12}|=2, |E_{4,13}|=1,$
$|E_{3,12}|=1$. Then, we have:
$NEC(A_6, x, y) = 2x^{11}y^{12} + x^9y^{11} + x^9y^9 + x^8y^{12} + x^8y^9 + 2x^7y^{13} + 2x^7y^{12} + x^4y^{13} + x^3y^{12}$.

Theorem 12 Let A_6 be oxypurinol graph. Taking Figure 2, various neighborhood eccentricity descriptors for the graph are calculated as:

i. $NE_1(A_6) = 231$ v. $NSDE(A_6) = 29.430$
ii. $NE_2(A_6) = 1050$ vi. $NISIE(A_6) = 53.364$
iii. $NFE(A_6) = 2407$ vii. $NHE(A_6) = 1.264$
iv. $NRE(A_6) = 20910$ viii. $NAE(A_6) = 1617.721$

Theorem 13. Let A_7 be topiroxostat graph. Then its neighborhood eccentricity polynomial is given as:

$$NEC(A_7, x, y) = x^{21}y^{25} + x^{20}y^{28} + 2x^{20}y^{20} + x^{19}y^{22} + x^{18}y^{28} + 2x^{18}y^{25} + 2x^{18}y^{20} + x^{18}y^{18} + x^{16}y^{28} + 2x^{16}y^{22} + x^{16}y^{18} + 2x^{13}y^{21} + 2x^{13}y^{19} + x^{13}y^{13} + x^{10}y^{20}.$$

Proof: Topiroxostat has |V|=19 and |E|= 21 and edge partition for it is mentioned as:
$|E_{21,25}|=1, |E_{20,28}|=1, |E_{20,20}|=1, |E_{19,22}|=1, |E_{18,28}|=1, |E_{18,25}|=2, |E_{18,20}|=2, |E_{18,18}|=1,$
$|E_{16,28}|=1, |E_{16,22}|=2, |E_{16,18}|=1, |E_{13,21}|=2, |E_{13,19}|=1, |E_{13,13}|=1, |E_{10,20}|=1$. Then, we have:

$$NEC(A_7, x, y) = x^{21}y^{25} + x^{20}y^{28} + 2x^{20}y^{20} + x^{19}y^{22} + x^{18}y^{28} + 2x^{18}y^{25} + 2x^{18}y^{20} + x^{18}y^{18} + x^{16}y^{28} + 2x^{16}y^{22} + x^{16}y^{18} + 2x^{13}y^{21} + 2x^{13}y^{19} + x^{13}y^{13} + x^{10}y^{20}.$$

Theorem 14 Let G be topiroxostat graph. Taking Figure 2, various neighborhood eccentricity descriptors for the graph are calculated as:

i. $NE_1(A_7) = 801$ v. $NSDE(A_7) = 44.405$
ii. $NE_2(A_7) = 7600$ vi. $NISIE(A_7) = 194.951$
iii. $NFE(A_7) = 16015$ vii. $NHE(A_7) = 1.127$
iv. $NRE(A_7) = 302098$ viii. $NAE(A_7) = 20963.380$

Table 2. Physical properties of gout drugs.

Drugs	BP	EV	FP	MR	PSA	Pol	ST	MV	C
Colchicine	726	106	392.9	106.6	83	–	42.3	50.5	740
Lesinurad	643.7	99.8	343.1	97.8	93	38.8	67	234	479
Allopurinol	–	1.816	–	34.7	75	13.8	126.4	80	190
Febuxostat	536.6	85.6	278.3	83.1	111	32.9	63.8	241	448
Prednisone	573.7	98.7	314.8	94.1	92	37.3	58.6	273.6	764
Oxypurinol	662.9	101	354.7	36.6	95	14.5	170.2	78.4	217
Probenecid	438	73.2	218.7	73.5	83	29.1	46.7	233.5	374
Methotrexate	–	–	–	119	211	47.2	96.5	295.7	704
Topiroxostat	594.7	88.6	175.3	65.9	91	26.1	100.2	170.9	344
Arhalofenate	551.1	83.1	287.1	95.9	65	38	39.8	312.3	524
Verinurad	566.7	89.5	296.5	99.6	99	39.5	71.5	259.9	541

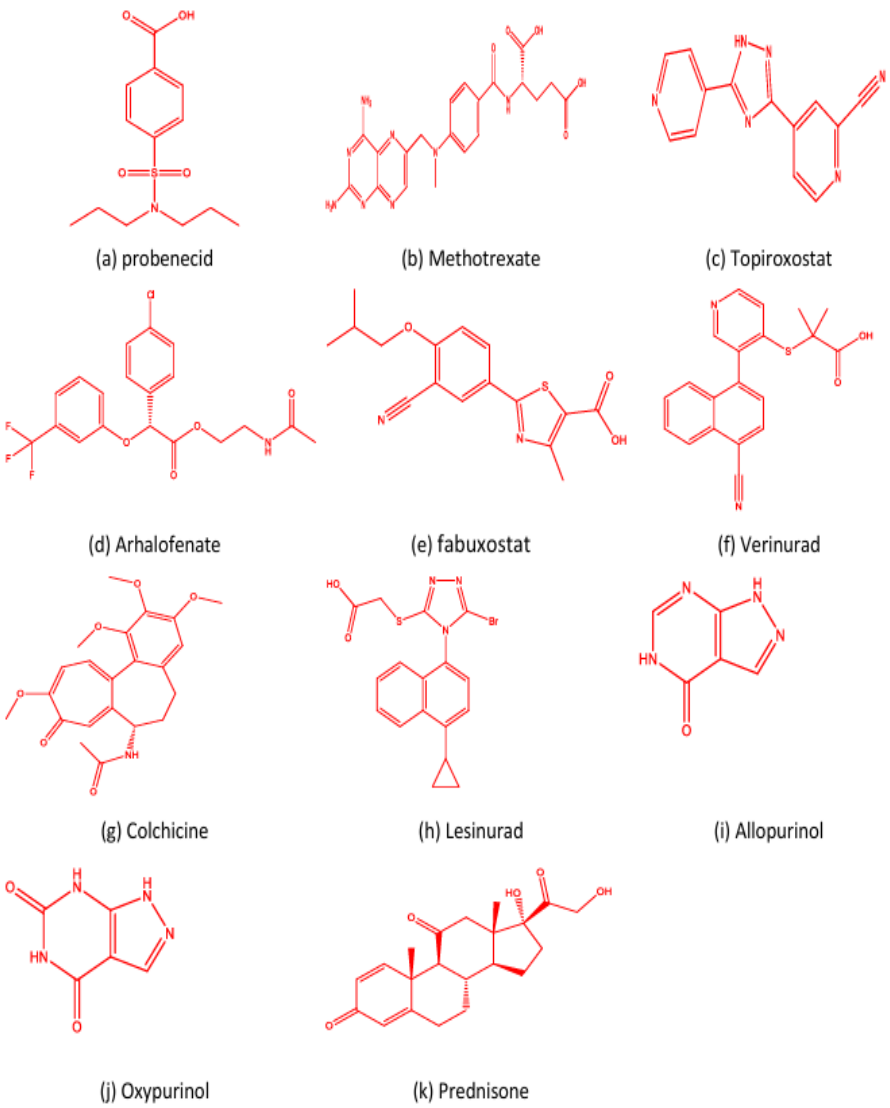

FIGURE 2. Gout treatment drugs.

Theorem 15. Let A_8 be a methotrexate graph. Then its neighborhood eccentricity polynomial is given as:

$$NECA_8, x, y) = 2x^{46}y^{49} + x^{46}y^{47} + x^{35}y^{40} + x^{34}y^{55} + 2x^{34}y^{53} + x^{34}y^{49} + x^{34}y^{47} + x^{32}y^{46} + x^{32}y^{34} + x^{31}y^{34} + x^{30}y^{47} + 2x^{28}y^{46} + 3x^{28}y^{40} + x^{28}y^{30} + x^{24}y^{40} + x^{24}y^{34} + 2x^{22}y^{35} + 2x^{21}y^{31} + 2x^{21}y^{22} + 2x^{18}y^{55} + x^{18}y^{53} + 3x^{16}y^{49} + x^{13}y^{40} + x^{11}y^{34}.$$

Proof: Methotrexate has |V|=33 and |E|= 35 and edge partition for it is mentioned as:

$|E_{46,49}|=2, |E_{46,47}|=1, |E_{35,40}|=1, |E_{34,55}|=1, |E_{34,53}|=2, |E_{34,49}|=1, |E_{34,47}|=1,$
$|E_{32,46}|=1, |E_{32,34}|=1, |E_{31,34}|=1, |E_{30,47}|=1, |E_{28,46}|=2, |E_{28,40}|=3, |E_{28,30}|=1, |E_{24,40}|=1,$
$|E_{24,34}|=1, |E_{22,35}|=2, |E_{21,31}|=2, |E_{21,22}|=2, |E_{18,55}|=2, |E_{18,53}|=1, |E_{16,49}|=3, |E_{13,40}|=1,$
$|E_{11,34}|=1$. Then, we have:

$$NEC(A_8,x,y) = 2x^{46}y^{49} + x^{46}y^{47} + x^{35}y^{40} + x^{34}y^{55} + 2x^{34}y^{53} + x^{34}y^{49} + x^{34}y^{47} + x^{32}y^{46} + x^{32}y^{34} + x^{31}y^{34} + x^{30}y^{47} + 2x^{28}y^{46} + 3x^{28}y^{40} + x^{28}y^{30} + x^{24}y^{40} + x^{24}y^{34} + 2x^{22}y^{35} + 2x^{21}y^{31} + 2x^{21}y^{22} + 2x^{18}y^{55} + x^{18}y^{53} + 3x^{16}y^{49} + x^{13}y^{40} + x^{11}y^{34}.$$

Theorem 16 Let A_8 be methotrexate graph. Taking Figure 2, various neighborhood eccentricity descriptors for the graph are calculated as:

i. $NE_1(A_8) = 2417$ v. $NSDE(A_8) = 84.320$
ii. $NE_2(A_8) = 40330$ vi. $NISIE(A_8) = 557.673$
iii. $NFE(A_8) = 93227$ vii. $NHE(A_8) = 1.060$
iv. $NRE(A_8) = 302707$ viii. $NAE(A_8) = 183027.43$

Theorem 17. Let A_9 be arhalofenate graph. Then its neighborhood eccentricity polynomial is given as:

$$NEC(A_9,x,y) = x^{34}y^{50} + x^{23}y^{25} + x^{23}y^{23} + x^{22}y^{37} + x^{22}y^{34} + x^{22}y^{22} + x^{20}y^{34} + 2x^{20}y^{32} + 2x^{20}y^{28} + 2x^{20}y^{22} + 2x^{18}y^{25} + 3x^{18}y^{20} + x^{16}y^{28} + 2x^{16}y^{23} + x^{16}y^{18} + 3x^{12}y^{50} + 2x^{12}y^{37} + x^{11}y^{32} + x^{7}y^{23}.$$

Proof: Arhalofenate has |V|=28 and |E|= 29 and edge partition for it is mentioned as:
$|E_{34,50}|=1, |E_{23,25}|=1, |E_{23,23}|=1, |E_{22,37}|=1, |E_{22,34}|=1, |E_{20,32}|=2, |E_{20,28}|=2, |E_{20,22}|=2,$
$|E_{18,25}|=2, |E_{18,20}|=3, |E_{16,28}|=1, |E_{16,23}|=1, |E_{16,18}|=1, |E_{12,50}|=3, |E_{12,37}|=2, |E_{11,32}|=1,$
$|E_{7,23}|=1$. Then, we have:

$$NEC(A_9,x,y) = x^{34}y^{50} + x^{23}y^{25} + x^{23}y^{23} + x^{22}y^{37} + x^{22}y^{34} + x^{22}y^{22} + x^{20}y^{34} + 2x^{20}y^{32} + 2x^{20}y^{28} + 2x^{20}y^{22} + 2x^{18}y^{25} + 3x^{18}y^{20} + x^{16}y^{28} + 2x^{16}y^{23} + x^{16}y^{18} + 3x^{12}y^{50} + 2x^{12}y^{37} + x^{11}y^{32} + x^{7}y^{23}.$$

Theorem 18 Let A_9 be arhalofenate graph. Taking Figure 2, various neighborhood eccentricity descriptors for the graph are calculated as:

i. $NE_1A_9 = 1388$ v. $NSDE(A_9) = 73.342$
ii. $NE_2(A_9) = 15463$ vi. $NISIE(A_9) = 310.948$
iii. $NFE(A_9) = 38810$ vii. $NHE(A_9) = 1.266$
iv. $NRE(A_9) = 812970$ viii. $NAE(A_9) = 47466.779$

Theorem 19. Let A_9 be Verinurad graph. Then its neighborhood eccentricity polynomial is given as:

$$NEC(A_{10},x,y) = x^{31}y^{38} + x^{25}y^{26} + x^{22}y^{25} + x^{20}y^{26} + 2x^{20}y^{22} + x^{20}y^{20} + x^{18}y^{25} + 2x^{18}y^{18} + x^{16}y^{38} + x^{16}y^{26} + 3x^{16}y^{22} + x^{16}y^{18} + 2x^{16}y^{16} + 2x^{14}y^{20} + 2x^{14}y^{16} + 2x^{10}y^{31} + x^{10}y^{20} + 2x^{9}y^{38}.$$

Proof: Verinurad has |V|=25 and |E|= 27 and edge partition for it is mentioned as:
$|E_{31,38}|=1, |E_{25,26}|=1, |E_{22,25}|=1, |E_{20,26}|=1, |E_{20,22}|=1, |E_{20,20}|=1, |E_{18,25}|=1, |E_{18,18}|=2,$
$|E_{16,38}|=1, |E_{16,26}|=1, |E_{16,22}|=3, |E_{16,18}|=1, |E_{16,16}|=2, |E_{14,20}|=2, |E_{14,16}|=2, |E_{10,31}|=2,$
$|E_{10,20}|=1, |E_{9,38}|=2$. Then, we have:

$$NEC(A_{10},x,y) = x^{31}y^{38} + x^{25}y^{26} + x^{22}y^{25} + x^{20}y^{26} + 2x^{20}y^{22} + x^{20}y^{20} + x^{18}y^{25} + 2x^{18}y^{18} + x^{16}y^{38} + x^{16}y^{26} + 3x^{16}y^{22} + x^{16}y^{18} + 2x^{16}y^{16} + 2x^{14}y^{20} + 2x^{14}y^{16} + 2x^{10}y^{31} + x^{10}y^{20} + 2x^{9}y^{38}.$$

Theorem 20 Let A_{10} be verinurad graph. Taking Figure 2, various neighborhood eccentricity descriptors for the graph are calculated as:

i. $NE_1(A_{10}) = 1094$ v. $NSDE(A_{10}) = 64.169$
ii. $NE_2(A_{10}) = 10668$ vi. $NISIE(A_{10}) = 253.411$
iii. $NFE(A_{10}) = 24928$ vii. $NHE(A_{10}) = 1.384$
iv. $NRE(A_{10}) = 472496$ viii. $NAE(A_{10}) = 30237.242$

Here we mention the technique to utilize the Table 1 formulas to obtain the results of the following sections. The neighborhood eccentricities descriptors are calculated as defined in subsection 2.1 and it values are tabulated in Table 3.

3.2. **CURVILINEAR REGRESSION ANALYSIS OF QSPR MODELS.** Nine physicochemical properties of medications are found at https://pubchem.ncbi.nlm.nih.gov/ and shown in the correlation coefficients (R) between the neighborhood eccentricity descriptors and pharmacological attributes, as established by linear, quadratic, cubic and bicubic regression models are shown in Table 4 to Table 7. Since R is greater than the critical value of 0.5 and p-value is less than 0.05 and the highest value of R indicates that features are statistically significant. For these computations, Pearson's correlation coefficient was employed [12]. The linear, quadratic, cubic and Bicubic regression models for different neighborhood eccentricity descriptors values are compared in Figure 5 to Fig 9. The regression equations in section 4 offer the most precise approximation for the physicochemical properties of the medications of gout drugs. To avoid lengthy computational details, only summarized results and concise data with the best regression models are presented in the manuscript.

Table 3. Neighborhood eccentric indices of gout drugs.

Drugs	NE_1	NE_2	NFE	NRE	NSD	NISIE	NHE	NAE
Colchicine	1206	11510	25338	476428	70.519	285.653	1.648	32034.961
Lesinurad	1096	10984	23858	473732	60.017	262.252	1.370	31966.926
Allopurinol	187	778	1683	13790	24.781	44.718	1.318	1164.642
Febuxostat	980	10022	23530	465762	55.488	224.957	1.131	29248.969
Prednisone	1308	14175	33666	711818	73.737	296.579	1.353	44303.755
Oxypurinol	231	1050	2407	20910	29.430	53.364	1.264	1617.721
Probenecid	665	5516	13143	210132	48.313	150.748	1.126	13637.523
Methotrexate	2417	40330	93227	302707	84.320	557.673	1.060	183027.430
Topiroxostat	801	7600	16015	302098	44.405	194.951	1.127	20963.380
Arhalofenate	1388	15463	38810	812970	73.342	310.948	1.266	47466.779
Verinurad	1094	10668	24928	472496	64.169	253.411	1.384	30237.242

3.3. **CURVILINEAR REGRESSION MODELS FOR GOUT DRUGS.** This section present a QSPR analysis utilizing Equation 1 to Equation 4 for linear, quadratic, cubic and bicubic regression models on applying NEC [30]. The authors discussed effective models based on neighborhood eccentricity descriptors that predict properties efficiently and are discussed below [35]. Most of the models are omitted due to page limitations. The linear and quadratic models detail is depicted in Table 4 and Table 5. Both the models show good correlation for MR, PSA, MV and C except ST. Some cubic regression models are given as under:

$$\text{PSA} = 1.08 \times 10^{-12} \cdot [\text{NFE}]^3 - 1.16 \times 10^{-7} \cdot [\text{NFE}]^2 + 2.85 \times 10^{-3} \cdot \text{NFE} + 76.7.$$

$$MV = 3.13 \times 10^{-15} \cdot [\text{NFE}]^3 - 3.95 \times 10^{-9} \cdot [\text{NFE}]^2 + 1.48 \times 10^{-3} \cdot NRE + 57.2.$$

$$MR = 1.10 \times 10^{-4} \cdot [\text{NSDE}]^3 - 2.97 \times 10^{-2} \cdot [\text{NSDE}]^2 + 3.57 \times 10^{0} \cdot NSDE - 40.9.$$

$$ST = 1.78 \times 10^{-3} \cdot [\text{NSDE}]^3 - 2.28 \times 10^{-1} \cdot [\text{NSDE}]^2 + 6.63 \times 10^{0} \cdot NSDE + 95.7.$$

$$C = -4.76 \times 10^{-3} \cdot [\text{NSDE}]^3 + 7.90 \times 10^{-1} \cdot [\text{NSDE}]^2 - 3.08 \times 10^{1} \cdot NSDE + 552.$$

$$Pol = 2.04 \times 10^{-7} \cdot [\text{NFE}]^3 - 3.03 \times 10^{-4} \cdot [\text{NFE}]^2 + 1.79 \times 10^{-1} \cdot NFE + 6.12.$$

$$PSA = -7.26 \times 10^{3} \cdot [\text{NAE}]^3 + 3.00 \times 10^{4} \cdot [\text{NAE}]^2 - 4.09 \times 10^{4} \cdot NAE + 18500.$$

4. COMPARISON OF CORRELATION COEFFICIENTS

Graph offer a succinct and efficient method of summarizing data, improving its presentation and readability. Additionally, graphs make it easier to compare various data sets which enable better decision making. Bar graphs in Figure 3 show how topological descriptors relation. The various correlations of the NEC descriptors are represented by distinct colors in each graph. For instance, the PSA correlation, which ranges from 0.990, is shown by orange. The strongest correlation range for the molar volume is 0.806. The correlation between the Molar refractivity and NEC that is shown in Figure 6 as a curve that falls 0.997 for NSDE, showing a good connection. A strong and significant correlation of 0.993 is shown polarity of graph. There is a remarkable range of findings from 0.806 in the graph between molar volume and NEC. Moreover, there is no connection between if correlation is greater than 0.05 and suggests that the association is weak. Figure 4 to Figure 8 show the relation among regression models linear to cubic models. The correlation coefficient of best models for afore mentioned properties in Table 6 and Table 7 are show as bold. Further the Figure 9 represents actual vs. predicted values of the said disease drugs.

Table 6 demonstrates that novel neighborhood eccentricity descriptors are the most accurate predictors for each attribute. It is clear from Table 3 to Table 7 that the features C and PSA are predicted by NED in cubic regression model whilst the remaining qualities are well predicted by the cubic model. Moreover, while the best predictor for the qualities MV and MR are the indices NRE and NSDE respectively. In addition to the key predictors, the statistical measurements including R^2, RMSE, p-value and F-Stat. Boiling point, flash point and density have not good correction for gout drugs with these descriptors.

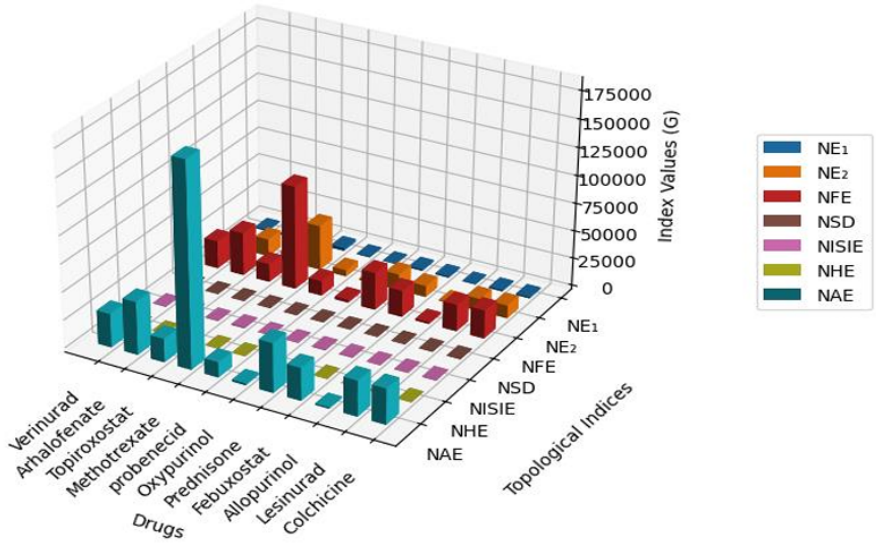

FIGURE 3. Comparisons of Neighborhood Eccentricity Descriptors.

Table 4. Linear Regression Models for characteristics of gout drugs.

Regression Equations with NE_1	R	R^2	SE	F-statistic	P
MR = 4.02 ×$10^{-2}$$NE_1$ + 40.9	0.894	0.799	12.95	35.733	0.0002
PSA = 4.55×$10^{-2}$$NE_1$ + 52.8	0.712	0.508	28.732	9.279	0.0139
Pol = 1.56×$10^{-2}$$NE_1$ + 15.9	0.911	0.83	4.535	43.932	0.0001
ST = -2.92×$10^{-2}$$NE_1$ + 11.1	0.444	0.197	37.872	2.209	0.1714
MV = 9.82×$10^{-2}$$NE_1$ + 10.1	0.641	0.41	75.521	6.261	0.0337
C = 2.65×$10^{-1}$$NE_1$ + 21.0	0.818	0.669	119.401	18.211	0.0021
Regression Equations with NE_2					
MR = 1.96×$10^{-3}$$NE_2$ + 59.6	0.763	0.583	18.652	12.564	0.0063
PSA = 3.08×$10^{-3}$$NE_2$ + 64.0	0.843	0.711	22.008	22.156	0.0011
Pol = 7.80×$10^{-4}$$NE_2$ + 22.9	0.796	0.633	6.661	15.538	0.0034
ST = -9.04×$10^{-4}$$NE_2$+ 90.8	0.24	0.058	41.03	0.55	0.4773
MV = 5.07×$10^{-3}$$NE_2$ + 144	0.578	0.334	80.249	4.515	0.0625
C = 1.27×$10^{-2}$$NE_2$ + 336	0.687	0.473	150.768	8.066	0.0194
Regression Equations with NFE					
MR = 8.40×$10^{-4}$$NFE + 59.8$	0.761	0.579	18.725	12.396	0.0065
PSA = 1.30×$10^{-3}$$NFE + 64.8$	0.829	0.687	22.911	19.746	0.0016
Pol = 3.35×$10^{-4}$$NFE + 23$	0.797	0.635	6.642	15.682	0.0033
ST = -4.06×$10^{-4}$$NFE + 91.2$	0.251	0.063	40.907	0.607	0.4559
MV = 2.26×$10^{-3}$$NFE + 142$	0.601	0.361	78.592	5.091	0.0505
C = 5.45×$10^{-3}$$NFE + 337$	0.687	0.472	150.858	8.046	0.0195
Regression Equations with NRE					
MR = 7.72×$10^{-5}$$NRE + 52.5$	0.71	0.505	20.317	9.175	0.0143
PSA = -2.09×$10^{-5}$$NRE + 108$	0.136	0.018	40.568	0.169	0.6909
Pol = 2.96×$10^{-5}$$NRE + 20.6$	0.715	0.511	7.694	9.392	0.0135
ST = -1.23×$10^{-4}$$NRE + 128$	0.773	0.598	26.793	13.394	0.0052
MV = 2.32×$10^{-4}$$NRE + 113$	0.627	0.393	76.593	5.836	0.0389
C = 5.56×$10^{-4}$$NRE + 269$	0.711	0.505	146.036	9.19	0.0142
RM of Properties with NSE					
MR = 1.40×10^{0}·NSE + 2.49	0.965	0.932	7.532	123.257	0.0000
PSA = 9.12×10^{-1}·NSE + 47.7	0.444	0.197	36.697	2.205	0.1717
Pol = 5.28×10^{-1}·NSE + 1.86	0.956	0.914	3.225	95.706	0.0000
ST = -1.43×10^{0}·NSE + 162	0.673	0.453	31.272	7.439	0.0233
MV = 3.20×10^{0}·NSE + 2.0	0.648	0.42	74.917	6.507	0.0311
C = 9.75×10^{0}·NSE - 72.9	0.935	0.875	73.477	62.855	0.0000

Table 5. Quadratic Regression Models for characteristics of gout drugs.

Regression Equations with NRE	R	R^2	SE	F-statistic	P
MR = -2.02×10^{-10}·$[NRE]^2$+ 2.35×10^{-4}·NRE + 33.2	0.868	0.754	15.186	12.265	0.003658
PSA = -2.40×10^{-10}·$[NRE]^2$ + 1.67×10^{-4}·NRE + 85	0.441	0.194	38.989	0.963	0.4219
Pol = -7.20×10^{-11}·$[NRE]^2$ + 8.60×10^{-5}·NRE + 13.7	0.854	0.73	6.063	10.807	0.005325
ST = 1.79×10^{-10}·$[NRE]^2$ - 2.63×10^{-4}·NRE + 145	0.83	0.689	24.987	8.875	0.009318
MV = -1.45×10^{-10}·$[NRE]^2$ + 3.46×10^{-4}·NRE + 98.8	0.636	0.405	80.487	2.718	0.1257
C = -9.55×10^{-10}·$[NRE]^2$ + 1.30×10^{-3}·NRE + 177	0.783	0.614	136.9	6.349	0.022314
Regression Equations with NSE					
MR = -1.17×10^{-2}·$[NSE]^2$ + 2.65×10^{0}·NSE - 27	0.976	0.952	6.716	79.16	5.35E-06
PSA = 5.43×10^{-2}·$[NSE]^2$ - 4.90×10^{0}·NSE + 185	0.64	0.41	33.356	2.781	0.121077
Pol = -4.28×10^{-3}·$[NSE]^2$ + 9.86×10^{-1}·NSE - 8.93	0.966	0.932	3.032	55.2	2.08E-05
ST = 6.28×10^{-2}·$[NSE]^2$ - 8.14×10^{0}·NSE + 320	0.849	0.72	23.715	10.293	0.006134
MV = -4.57×10^{-2}·$[NSE]^2$ + 8.08×10^{0}·NSE – 95.1	0.668	0.446	77.651	3.217	0.094343
C = 9.16×10^{-3}·$[NSE]^2$ + 8.77×10^{0}·NSE - 498	0.935	0.875	77.86	27.996	0.000244
Regression Equations with NISIE					
MR = -3.62×10^{-4}·$[NISIE]^2$ + 3.83×10^{-1}·NISIE + 17.8	0.97	0.942	7.403	64.44	1.17E-05
PSA = 7.81×10^{-4}·$[NISIE]^2$ - 2.47×10^{-1}·NISIE + 100	0.912	0.832	17.803	19.805	0.000797
Pol = -1.25×10^{-4}·$[NISIE]^2$ + 1.40×10^{-1}·NISIE + 7.97	0.971	0.943	2.795	65.663	1.09E-05
ST = 1.05×10^{-3}·$[NISIE]^2$ - 7.26×10^{-1}·NISIE + 175	0.852	0.727	23.434	10.638	0.005576
MV = -8.23×10^{-4}·$[NISIE]^2$ + 8.87×10^{-1}·NISIE + 52.1	0.67	0.448	77.465	3.252	0.092548
C = -2.38×10^{-3}·$[NISIE]^2$ + 2.51×10^{0}·[NISIE] + 60.4	0.884	0.782	102.771	14.365	0.002251
Regression Equations with NHE					
MR = 3.32×10^{2}·$[NHE]^2$ - 8.60×10^{2}·NHE + 632	0.446	0.199	27.408	0.993	0.411798
PSA = 5.10×10^{2}·$[NHE]^2$ - 1.47×10^{3}·NHE + 1130	0.646	0.417	33.154	2.864	0.115327
Pol = 9.01×10^{1}·$[NHE]^2$ - 2.40×10^{2}·NHE + 189	0.297	0.088	11.14	0.387	0.691303
ST = -2.96×10^{2}·$[NHE]^2$ + 7.36×10^{2}·NHE - 368	0.346	0.12	42.057	0.545	0.600175
MV = -5.07×10^{2}·$[NHE]^2$ + 1.10×10^{3}·NHE - 359	0.5	0.25	90.324	1.334	0.316206
C = 2.37×10^{3}·$[NHE]^2$ - 5.94×10^{3}·NHE + 4150	0.527	0.278	187.133	1.539	0.271987
Regression Equations with NAE					
MR = -7.65×10^{-9}·$[NAE]^2$ + 1.83×10^{-3}·NAE + 39.1	0.928	0.861	11.435	24.687	0.000378
PSA = 4.75×10^{-9}·$[NAE]^2$ - 2.12×10^{-4}·NAE + 90	0.944	0.89	14.372	32.527	0.000144
Pol = -2.85×10^{-9}·$[NAE]^2$ + 6.94×10^{-4}·NAE + 15.5	0.946	0.894	3.797	33.767	0.000126
ST = 1.39×10^{-8}·$[NAE]^2$ - 2.75×10^{-3}·NAE + 136	0.811	0.657	26.24	7.674	0.013781
MV = -2.05×10^{-8}·$[NAE]^2$ + 4.89×10^{-3}·NAE + 87.5	0.722	0.521	72.159	4.358	0.052463
C = -5.45×10^{-8}·$[NAE]^2$ + 1.28×10^{-2}·NAE + 186	0.8735	0.763	107.2023	12.8778	0.003155

Table 6. Comparison between correlation coefficients of cubic and Bicubic regression analysis.

	Cubic Model			Bicubic Model		
	R	R^2	SE	R	R^2	SE
Regression Equations with NE_1						
MR	0.97	0.941	7.976	0.987	0.975	7.986
PSA	0.956	0.914	13.582	0.986	0.973	24.14
Pol	0.974	0.949	2.809	0.979	0.958	3.924
ST	0.862	0.743	24.297	0.934	0.873	51.327
MV	0.695	0.483	80.187	0.802	0.642	76.319
C	0.907	0.822	99.321	**0.982**	0.964	47.198
Regression Equations with NE_2						
MR	0.962	0.925	8.988	0.982	0.964	23.152
PSA	0.964	0.929	12.399	0.977	0.955	48.82
Pol	0.971	0.943	2.966	0.98	0.96	9.142
ST	0.854	0.729	24.947	0.885	0.783	82.888
MV	0.711	0.505	78.44	0.799	0.638	89.261
C	0.88	0.775	111.613	0.974	0.948	160.38
Regression Equations with NFE						
MR	0.964	0.929	8.716	0.978	0.957	26.265
PSA	**0.965**	0.931	12.192	0.98	0.96	52.743
Pol	**0.975**	0.951	2.759	0.981	0.962	10.593
ST	0.864	0.747	24.115	0.882	0.778	86.508
MV	0.739	0.547	75.083	0.799	0.639	109.817
C	0.873	0.761	115.007	0.957	0.915	133.461
Regression Equations with NRE						
MR	0.876	0.767	19.646	0.879	0.772	18.972
PSA	0.485	0.235	50.445	0.721	0.52	44.375
Pol	0.871	0.758	7.671	0.876	0.768	6.417
ST	0.849	0.721	70.968	**0.988**	0.975	81.895
MV	**0.748**	0.559	73.627	0.765	0.585	56.494
C	0.787	0.619	160.156	0.835	0.698	167.122

Table 7. Comparison between correlation coefficients of cubic and Bicubic regression analysis.

	Cubic Model			Bicubic Model		
	R	R^2	SE	R	R^2	SE
Regression Equations with NSDE						
MR	**0.976**	0.952	7.149	**0.997**	0.994	3.39
PSA	0.879	0.773	22.13	0.979	0.958	12.56
Pol	0.969	0.939	3.068	**0.993**	0.986	1.95
ST	**0.878**	0.771	22.934	0.965	0.932	16.55
MV	0.699	0.488	79.778	0.803	0.645	87.89
C	**0.943**	0.89	78.034	0.949	0.9	98.62
Regression Equations with NISIE						
MR	0.97	0.942	7.914	0.990	0.98	5.26
PSA	0.956	0.914	13.623	**0.990**	0.979	16.39
Pol	**0.972**	0.944	2.938	0.979	0.959	2.78
ST	0.854	0.729	24.964	0.95	0.903	40.6
MV	0.687	0.472	80.995	0.757	0.573	82.44
C	0.909	0.826	98.21	0.956	0.914	84.47
Regression Equations with NHE						
MR	0.717	0.515	22.81	0.841	0.707	23.46
PSA	0.922	0.85	17.963	0.978	0.957	12.78
Pol	0.688	0.473	9.053	0.826	0.683	9.29
ST	0.35	0.123	44.883	0.568	0.323	52.16
MV	0.656	0.43	84.162	0.757	0.573	96.36
C	0.723	0.522	162.741	0.828	0.686	174.53
Regression Equations with NAE						
MR	0.96	0.921	16.515	0.988	0.976	33.69
PSA	**0.965**	0.931	38.652	0.975	0.951	56.04
Pol	0.97	0.94	6.471	0.987	0.973	13.47
ST	0.841	0.707	72.426	0.909	0.826	81.94
MV	0.723	0.522	83.496	**0.806**	0.649	118.82
C	0.875	0.765	134.03	0.952	0.907	177.17

The effectiveness of three regression models linear (pink), quadratic (yellow dashed), and cubic (green dash-dot) in capturing the connections between physicochemical attributes and molecular descriptors across eight QSPR models was evaluated. The discussion for graphical analysis for some of the curvilinear regression analysis curves for Figure 4 to Figure 7 graphs is given as under:

i. Complexity vs. NAE: Figure 4 shows the linear model completely missed the curve by drawing a straight upward line, overestimating in the middle and underestimating at the ends. At high NAE, the quadratic model saw an implausible decline after experiencing some initial growth. The cubic model traced S-curve with a fast ascent, a plateau that flattened, and a moderate classic saturation behavior fitted the data the best.

ii. Density vs. NE_2: Figure 4 shows the data is disorganized and dispersed. It has a slight downward movement in the linear model. After forming a U-shape with a bottom at $NE_2 \approx 20,000$, the quadratic model moved up too sharply.

iii. Molar Refractivity vs. NAE: Figure 5 shows the linear trend continued to rise gradually. The quadratic model formed a hill with a top close to NAE $\approx$ 170 million; the middle was absent, but the ends matched. The cubic model over fitted once more, swinging sharply and plunging to a deep trough close to NAE $\approx$ 120 million.

iv. Flash Point vs. NRE: Figure 5 shows the linear model was ineffective for scattered locations and only slightly inclined upward. At the end, the quadratic model jumped after remaining flat. The cubic model over fitted to scattered data, oscillating wildly and collapsing after reaching a deep low close to NRE $\approx 200,000$.

v. Surface Tension vs. NE_1: Figure 7 shows the linear model sat above most locations but gradually decreased. The quadratic model tracked mid-range values well, curving into a U shape and bottoming close to $NE_1 \approx 1,300$. The quadratic model was enough and the cubic model nearly overlapped it, offering little benefit. It missed highs and lows, the linear model increased progressively. At high NAE, the quadratic model failed because to a little upward curvature. Severe over fitting was shown when the cubic model fell into negative values in the middle of the range and subsequently sky rocketed physically ridiculous for surface area.

vi. Boiling Point vs. NE_1: Figure 4 shows the linear model predicted roughly the same boiling point everywhere and was almost flat. The quadratic model missed an outlier around 740 but declined somewhat around $NE_1 \approx 1,000$. Completely over fitting, the cubic model reached negative boiling points.

vii. Molar Volume vs. NISIE: Figure 6 shows the linear model rose significantly. The quadratic model incorrectly dropped after arching downward and peaking close to NISIE $\approx 500,000$. The cubic model best matched the real pattern by tracing an S-curve with a sharp beginning plateaus, and upturns. When data followed saturation curves, cubic models performed exceptionally well for Complexity NAE and Molar Volume NISIE.

viii. Surface Tension vs. NE_1: Figure 7 shows quadratic and cubic is tied. Due to dispersed, sparse, or irregular data, all models for the other parameters density, molar refractivity, flash point, polar surface area, and boiling point struggled, with cubic models frequently over fitting into forecasts that were physically impossible.

Cubic models excelled for complexity NAE and Molar Volume NISIE where data followed saturation curves. Quadratic and cubic

tied for Surface Tension NE_1. For the rest Density, Molar Refractivity, Flash Point, Polar Surface Area, and Boiling Point all models often physically difficult for predictions. In the same manner other graph can be evaluated and it can be verified from the R^2 values form Table 4 to Table 7. The polynomial of degree six data does not efficient to predict the properties.

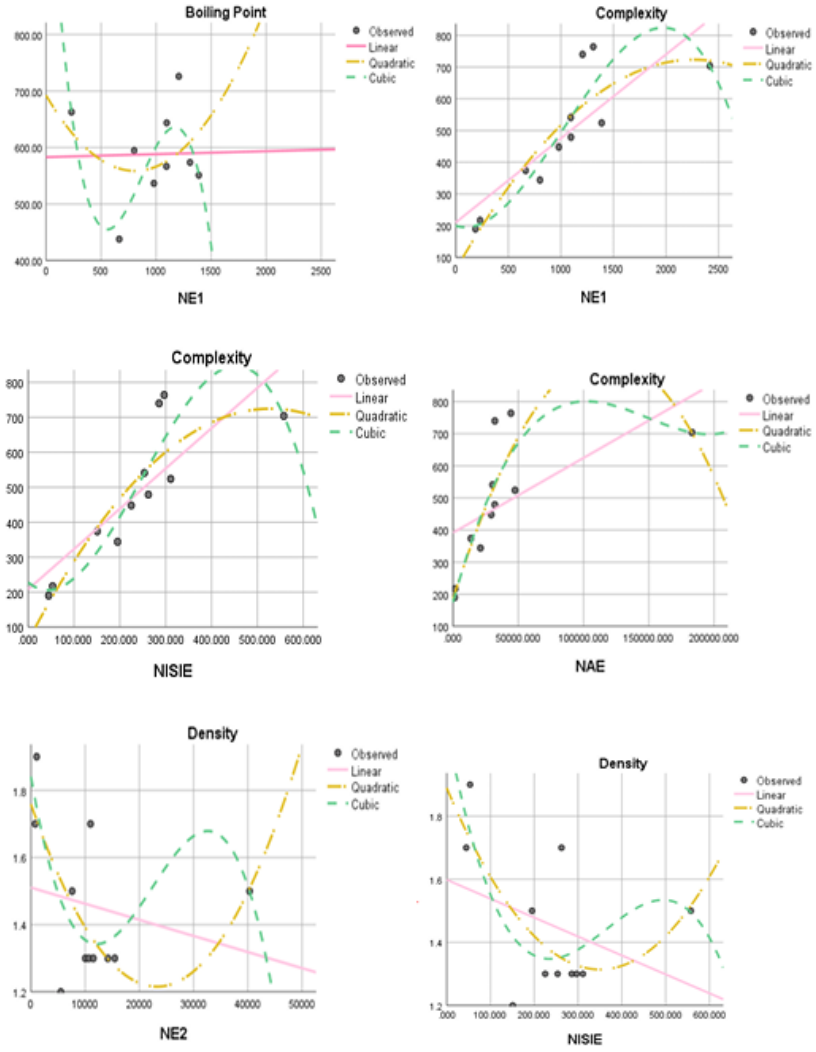

FIGURE 4. Comparison of linear, quadratic and cubic models.

5. RANDOM FOREST MODEL PERFORMANCE

An ensemble machine learning system called random forest (RF) uses several decision trees to get better prediction results. This method generates multiple decision trees from a random bootstrap sample of the records and only takes into account

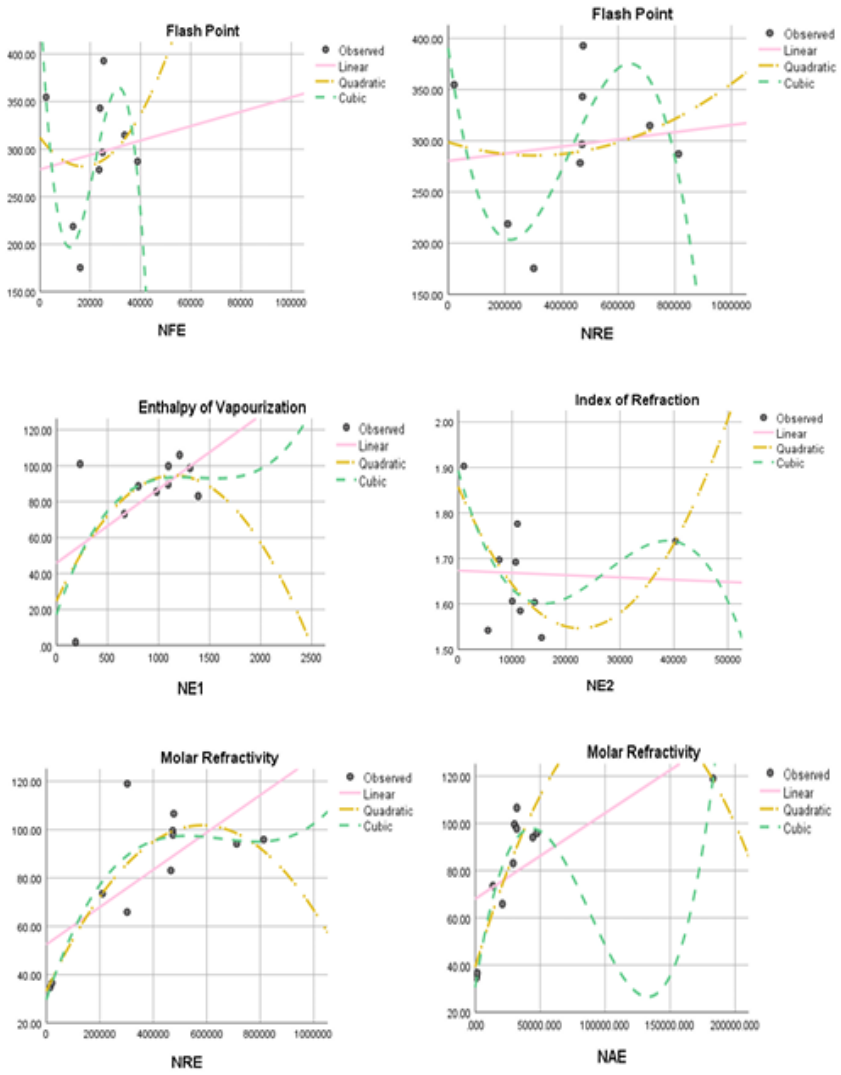

FIGURE 5. Comparison of linear, quadratic and cubic models.

a random subset of features at each split [43]. The average of the predictions from each individual tree is used to determine the final prediction for regression tasks. Key parameters include the number of trees, features considered at each split and tree depth constraints. Random forest is useful for figuring out which chemical descriptors influence property predictions since it naturally generates feature relevance scores. The output error metrics provided in Table 9 include mean absolute error (MAE), root mean squared error (RMSE), mean percentage error (MPE) and mean absolute percentage error (MAPE), which are commonly used measurements of model accuracy. The formulas for each metric are provided below.

i. $RMSE = \frac{1}{n}\sqrt{\sum(\text{actual} - \text{predicted})^2}$

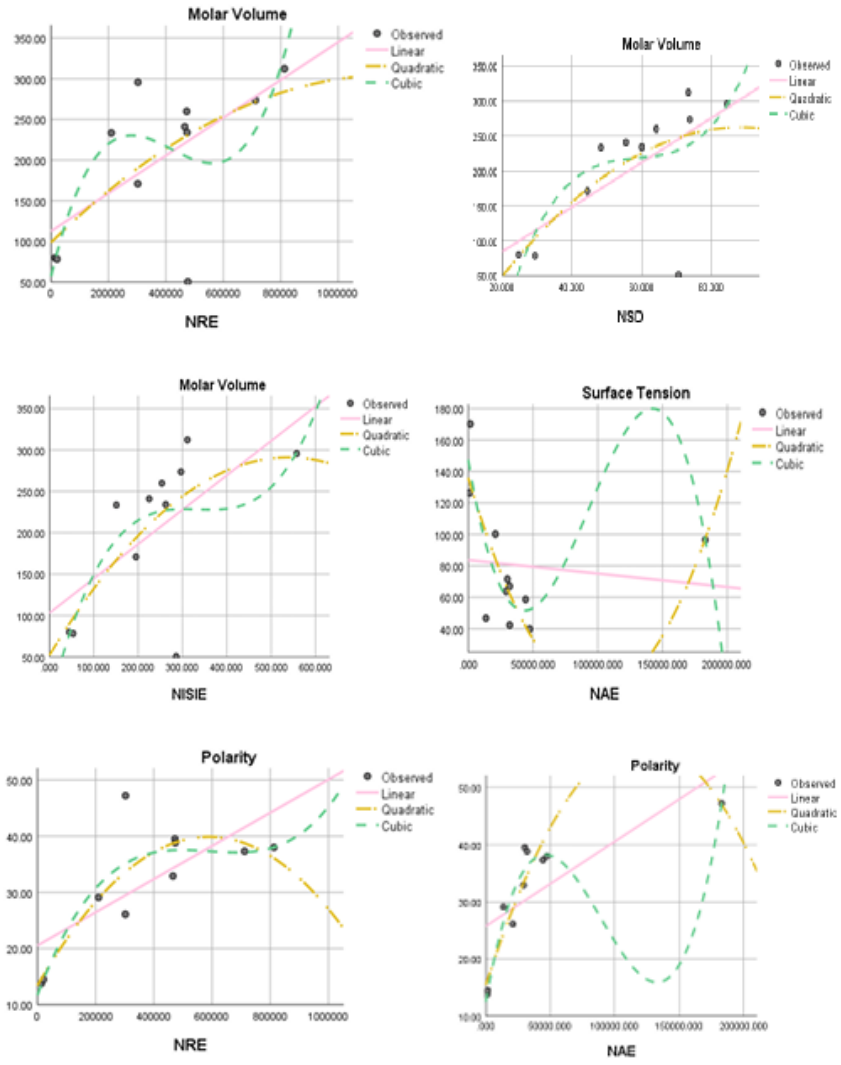

FIGURE 6. Comparison of linear, quadratic and cubic models.

ii. $MAE = \frac{1}{n}\sum|\text{actual} - \text{predicted}|$
iii. $MPE = \frac{100}{n}\sum\frac{\text{actual}-\text{predicted}}{\text{actual}}$
iv. $MAPE = \frac{100}{n}\sum\left|\frac{\text{actual}-\text{predicted}}{\text{actual}}\right|$

Random Forest provides advantages over conventional regression techniques in our LOOCV study comparing models for molecular property prediction (FP, BP, EV, MR, Pol, PSA, ST, MV and C). Without the need for feature scaling or human

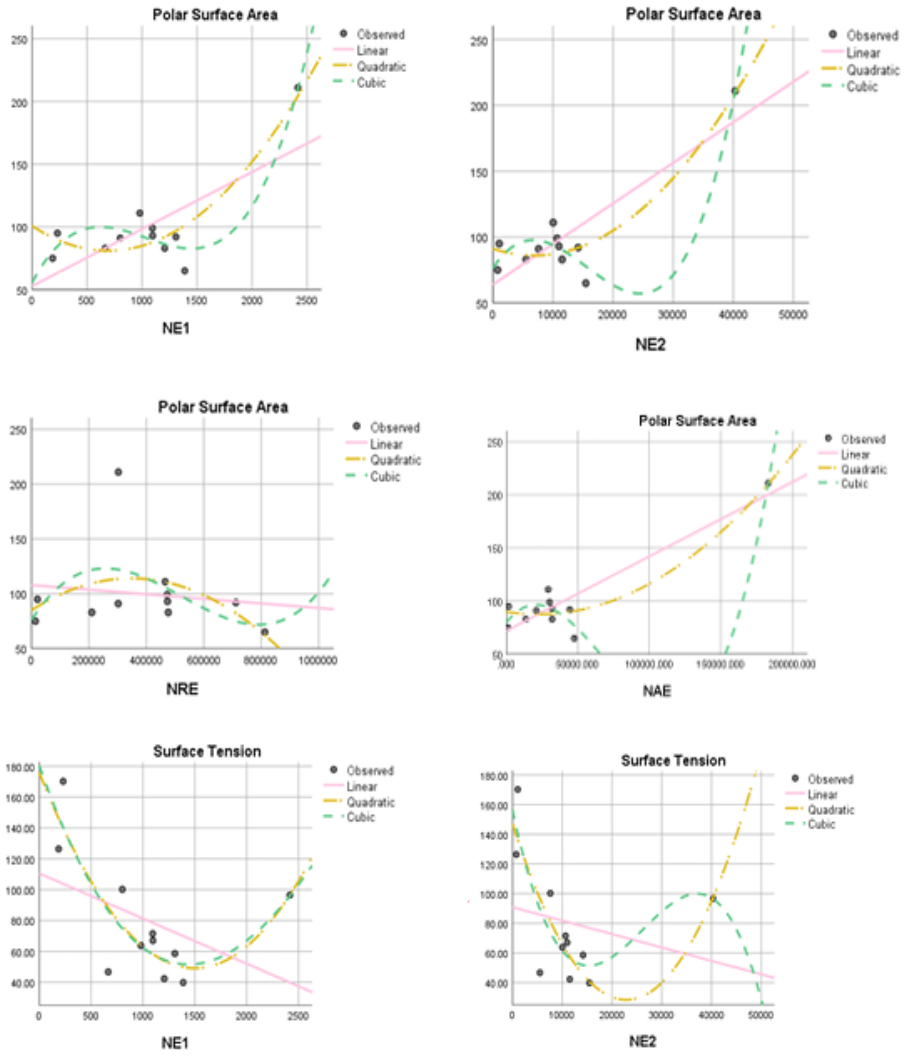

FIGURE 7. Comparison of linear, quadratic and cubic models.

interaction term specification, it automatically captures intricate non-linear interactions. For chemical data, where molecular descriptors frequently have non-linear relationships with target qualities, this is very helpful. Additionally, random forest's bootstrap aggregation process effectively manages sample sizes and shows resilience to outliers.

An objective performance assessment is provided by the model's integrated LOOCV and feature importance analysis. It will identify the molecular descriptors (NE, NE, NFE, NRE, NSD, NISIE, NHE and NAE) have the greatest impact on each prediction of the said properties. Because of these features, random forest serves as a potent benchmark against curvilinear regression models and advanced machine learning techniques in the forecast of drugs properties. The error measurement found in Table 9 and predicted values are mentioned in Table 8. For all gout drugs the predicted values are visualized in Figure 8 to Figure 12.

Python (Version 3.x) was used in a scientific computing environment for all machine learning experiments. We used the NumPy and Pandas libraries to reprocess the molecular descriptors and physicochemical property data sets and the scikit-learn standard utility was used to scale the features. Matplotlib was used to create a visualization of the experimental versus predicted values.

Table 8. Error measurement through Random Forest.

Property	R^2	MSE	RMSE	MAE	MPE (%)	MAPE (%)
FP	0.899689	405.0649	20.12622	15.26467	1.122315	5.313077
MR	0.981046	11.43247	3.381193	2.9445	-1.88717	4.645329
PSA	0.765927	49.51135	7.03643	5.856364	-0.00937	6.589744
Pol	0.918193	247.8504	15.74327	6.4717	-2.85662	9.057716
ST	0.936099	96.93196	9.845403	7.666545	-4.13506	11.85535
MV	0.852768	1164.964	34.13157	23.74282	-18.4195	26.1055
C	0.940315	2104.876	45.87892	35.79818	-2.8076	7.471678

Table 9. Predicted drugs properties through Random Forest.

Drugs	BP	EV	FP	MR	PSA	Pol	ST	MV	C
Colchicine	669.099	100.48	357.668	101.925	88.45	38.424	53.248	146.061	654.45
Lesinurad	610.579	96.351	325.525	97.168	94.68	38.114	66.118	228.09	514.27
Allopurinol	596.729	29.102	304.064	38.745	79.55	16.406	131.732	89.113	217.63
Febuxostat	548.275	85.864	269.243	86.834	103.3	35.53	60.668	241.303	471.67
Prednisone	596.919	95.876	322.465	95.671	86.55	37.699	53.528	264.62	689.32
Oxypurinol	596.008	69.452	302.658	38.894	88.02	16.394	150.12	89.349	225.28
Probenecid	495.552	76.645	213.434	71.455	86.28	29.531	61.373	216.415	367.91
Methotrexate	529.201	82.431	239.155	90.725	105.73	161.62	49.399	289.467	687.95
Topiroxostat	561.67	85.339	194.008	69.924	91.09	29.259	87.356	189.125	359.69
Arhalofenate	576.114	86.811	304.644	95.439	75.1	37.831	45.63	286.019	605.32
Verinurad	583.735	92.803	309.461	97.331	96.38	38.568	67.741	234.807	541.92

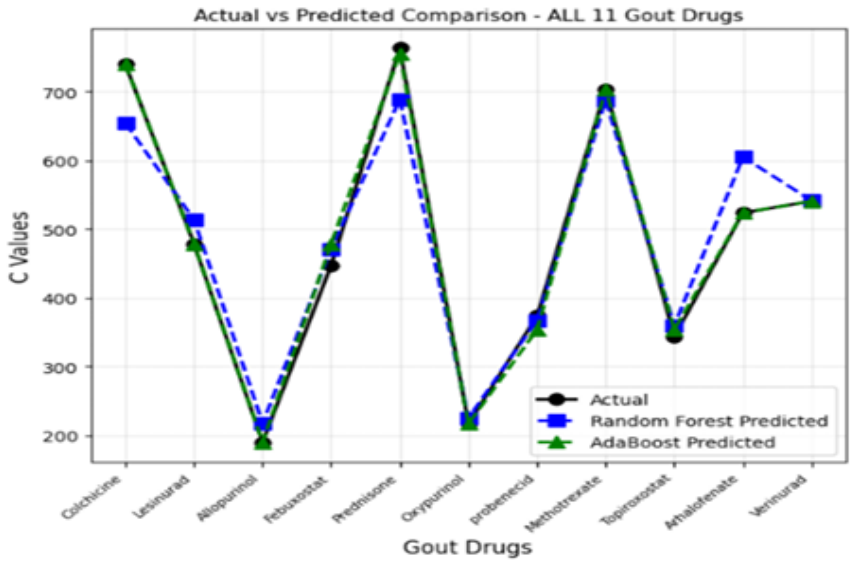

FIGURE 8. Graphical Comparison of Complexity.

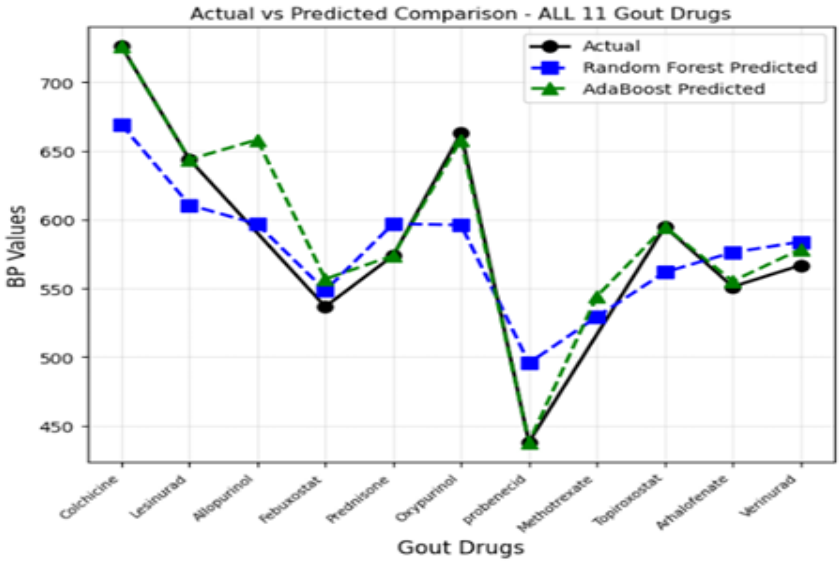

FIGURE 9. Graphical Comparison of Boiling Point .

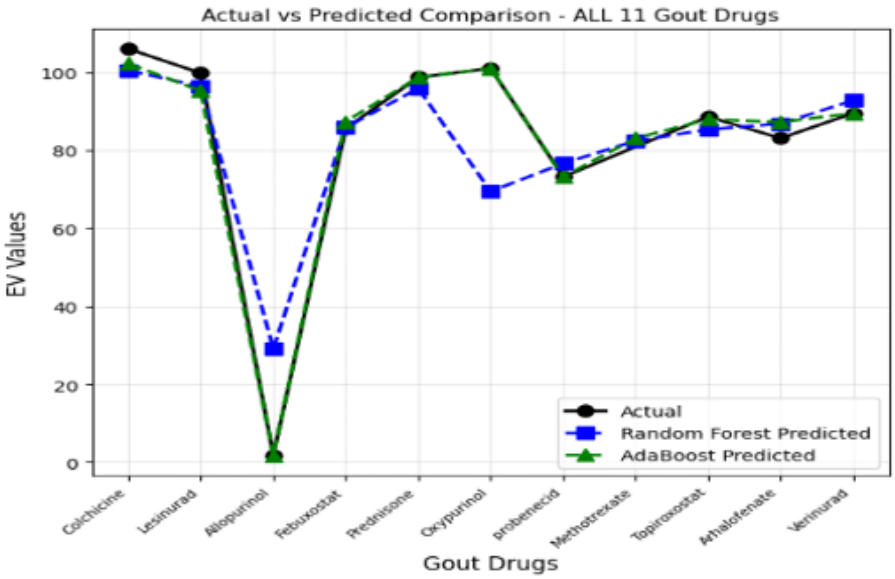

FIGURE 10. Graphical Comparison of Enthalpy of Vaporization.

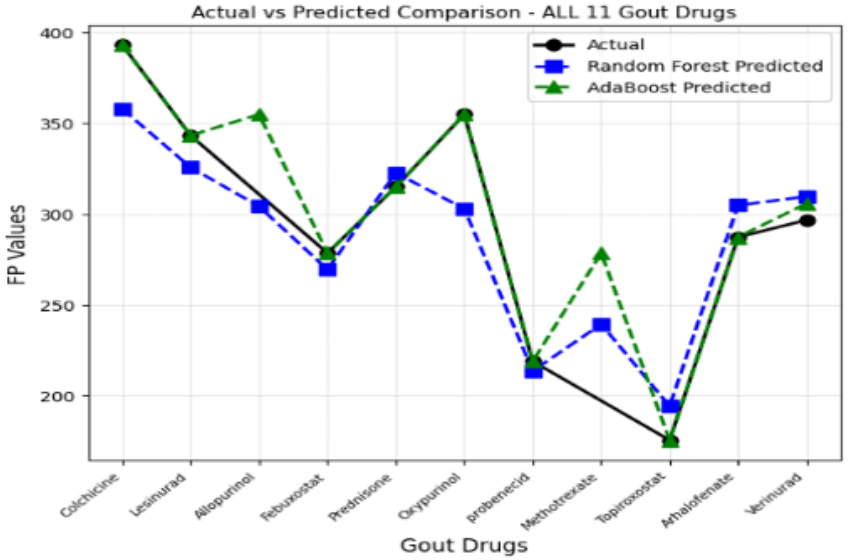

FIGURE 11. Graphical Comparison of Flash Point.

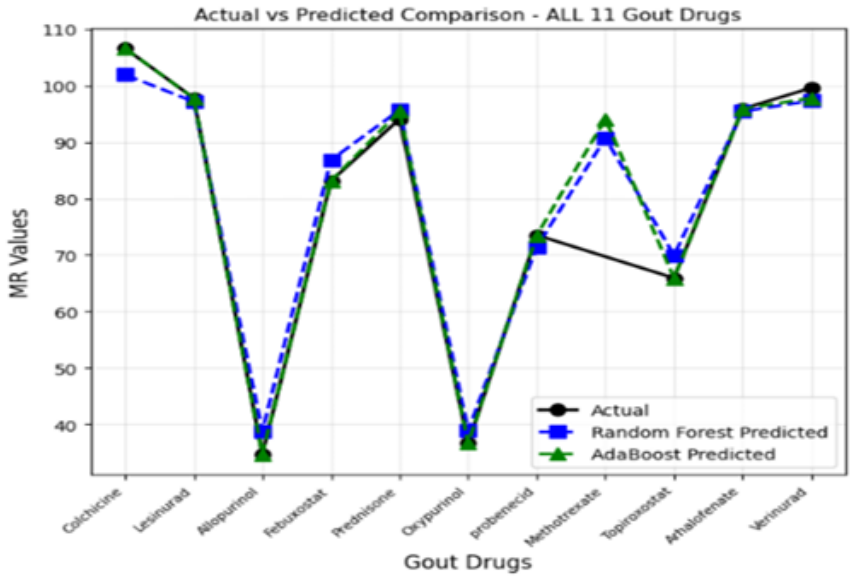

FIGURE 12. Graphical Comparison of Molar Refractivity.

6. ADABOOST MODEL PERFORMANCE

Adaboost is an ensemble learning technique. It constructs a resilient prediction model. It increases the weights of incorrectly predicted samples while decreases the weights of correctly predicted samples after training each weak. For regression the final prediction is a weighted average of all the guesses made by weak learners; learners that make fewer mistakes are given larger weights. Adaboost can create very accurate models by using this adaptive weighting technique [40]. The method provides distinct advantages as a boosting substitute for Random Forest's bagging strategy in our LOOCV study comparing models for chemical property prediction. Because each new learner fixes prior mistakes, Adaboost frequently generates lower bias than bagging algorithms, possibly exposing minute patterns in the chemical data.

When specific molecular descriptors (FP, BP, EV, MR, Pol, PSA, ST, MV and C) have intricate, conditional interactions with target attributes, this sequential error may be very helpful and found in Table 11. However, because Adaboost actively concentrates on challenging samples, it is more susceptible to noisy data and outliers than RF. When sample sizes are small, this could result in over fitting. The predicted values are mentioned in Table 10. For all gout drugs the predicted values are visualized in Figure 13 to Figure 16.

Table 10. Predicted drugs properties through Adaboost.

Drugs	BP	EV	FP	MR	PSA	Pol	ST	MV	C
Colchicine	726	102.25	392.9	106.6	83	38.4	42.3	50.5	740
Lesinurad	643.7	95.25	343.1	97.8	93.62	38.5	66.2	234	479
Allopurinol	658.1	1.816	354.7	34.7	75	13.8	126.4	80	190
Febuxostat	556.66	87.36	278.3	83.1	111	32.9	63.8	234	479
Prednisone	573.7	98.7	314.8	95.45	92	38	58.6	273.6	756
Oxypurinol	658.1	101	354.7	36.6	92.333	14.5	170.2	78.4	217
Probenecid	438	73.2	218.7	73.5	83	29.1	46.7	233.5	354
Methotrexate	544.125	83.1	278.3	94.1	119	211	46.7	295.7	704
Topiroxostat	594.7	87.98	175.3	65.9	91	27.6	100.2	170.9	354
Arhalofenate	555.15	87.22	287.1	95.9	65	38	42.3	312.3	524
Verinurad	578.366	89.5	305.65	97.8	95.5	38.5	66.366	250.45	541

Table 11. Error measurement through Adaboost.

Property	R^2	MSE	RMSE	MAE	MPE (%)	MAPE (%)
FP	0.999998	0.01	0.1	0.033333	-0.01161	0.01161
MR	0.999329	0.405	0.636396	0.27	-0.10092	0.281647
PSA	0.961323	8.180994	2.860244	1.350649	-0.43487	1.523816
Pol	0.999899	0.306951	0.554032	0.3275	-0.04782	0.968686
ST	0.997363	3.999798	1.999949	0.969697	0.507216	1.64929
MV	0.998864	8.988384	2.998063	1.354545	0.292486	0.663544
C	0.995908	144.3239	12.01349	6.522727	0.166529	1.424646

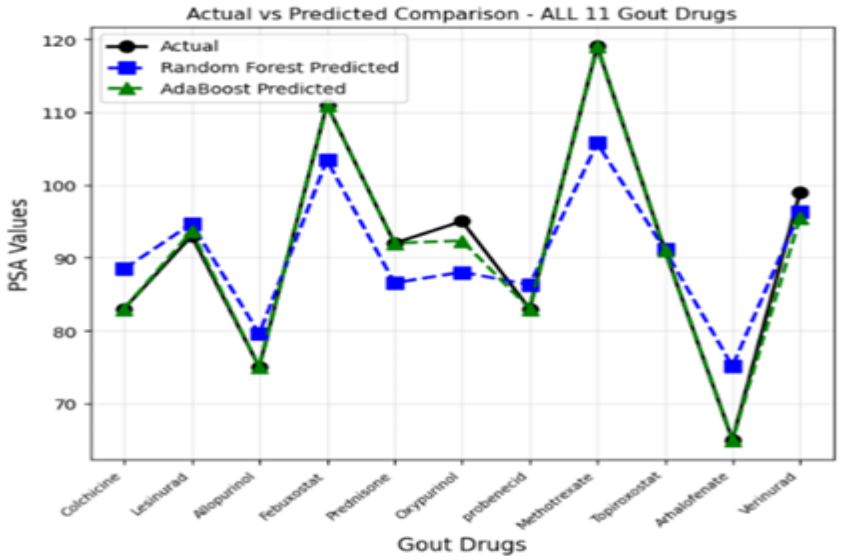

FIGURE 13. Graphical Comparison of Polar Surface Area.

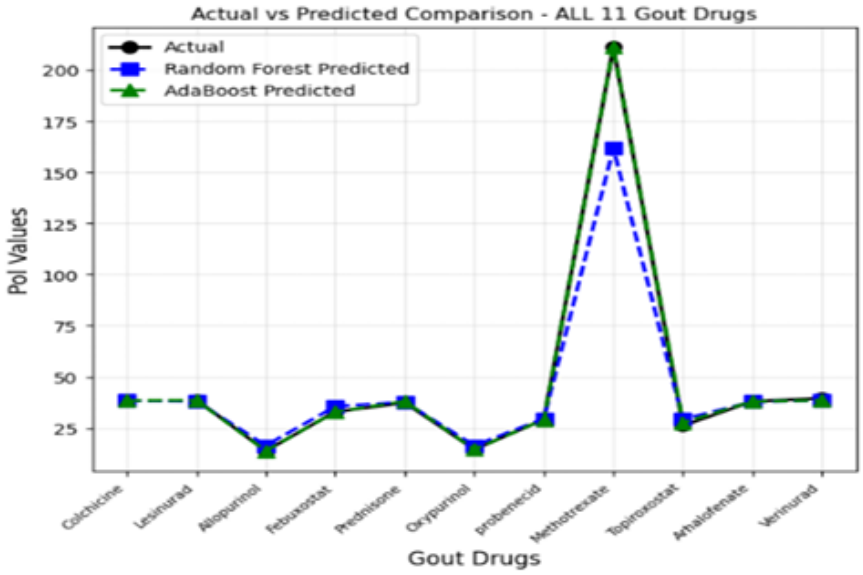

FIGURE 14. Graphical Comparison of Polarity.

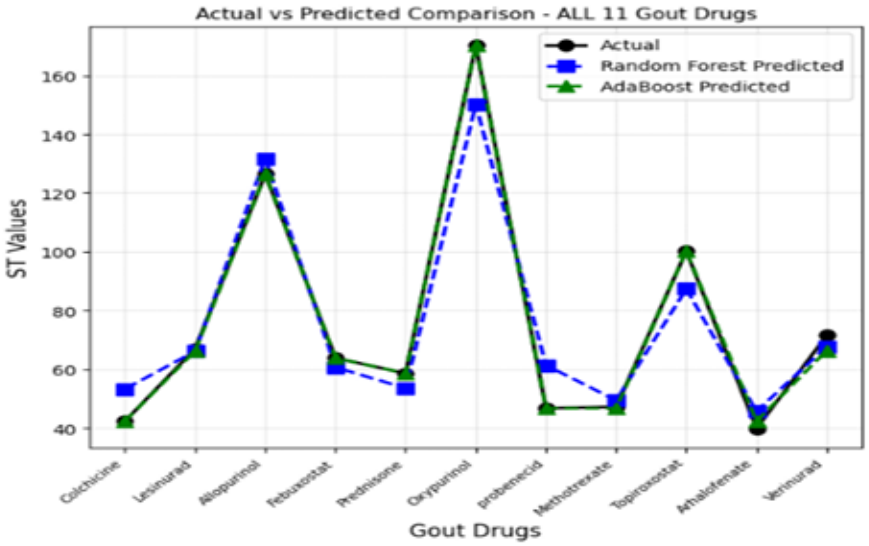

FIGURE 15. Graphical Comparison of Surface Tension.

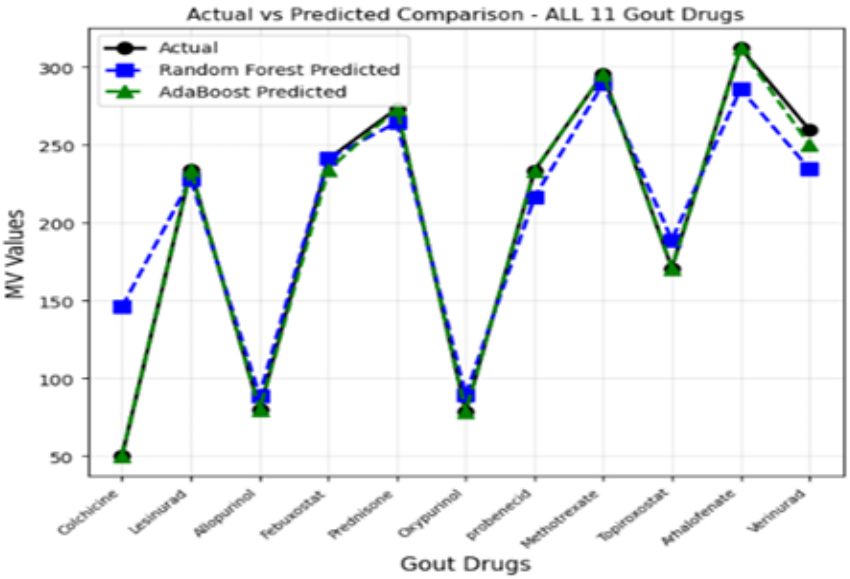

FIGURE 16. Graphical Comparison of Molar Volume.

Table 12. Comparison between correlation coefficients of RF and Adaboost regression analysis.

Property	MAE		MSE		RMSE		R^2	
	RF	Adaboost	RF	Adaboost	RF	Adaboost	RF	Adaboost
BP	36.0487	4.5093	1644.854	64.2472	40.5568	8.0154	0.7307	0.9895
EV	8.4611	1.4808	183.7367	5.5282	13.5549	2.3512	0.7745	0.9932
FP	19.5611	1.0167	583.6472	9.3025	24.1588	3.05	0.8555	0.9977
MR	2.575	0.315	8.6026	0.5063	2.933	0.7115	0.9857	0.9992
PSA	5.5527	0.6174	44.1178	1.7956	6.6421	1.34	0.7914	0.9915
Pol	6.2282	0.35	246.6977	0.383	15.7066	0.6189	0.9186	0.9999
ST	7.7039	0.8121	92.7915	3.0446	9.6328	1.7449	0.9388	0.998
MV	20.3395	1.4955	1039.433	12.573	32.2402	3.5458	0.8686	0.9984
C	34.1045	6.2727	2062.434	138.6364	45.414	11.7744	0.9415	0.9961

The error measures that can be shown to provide significant insights when evaluating the efficacy of prediction models like Random Forest and adaboost include MAE, MSE, RMSE and R^2, as shown in Figs. 17, 18 and 19 and Table 12. Comparing the efficacy is made simple by bar graphs among the models. After analyzing the data, it is clear that Adaboost outperforms Random Forest algorithm in terms of prediction efficiency, as evidenced by lower MAE, MSE, and Root RMSE and higher R^2.This illustration demonstrates how Adaboost efficiency is a potent method for predictive modeling applications since it makes better predictions with small errors.

7. MODEL VALIDATION AND PERFORMANCE EVALUATION

The robustness of random forest, Adaboost and curvilinear regression models was thoroughly evaluated over all examined parameters via LOOCV Table 13 and Table 14. Strongly negative R^2 results, high RMSE and MAE, and large MAPE tenets demonstrate curvilinear regression model's (Linear, quadratic, cubic and bicubic) have poor generalization ability for each target. Large MPE values show significant bias and erratic predictions, demonstrating that straightforward linear connections are insufficient to capture the intricate interaction between physicochemical attributes and molecular descriptors. The cubic regression model performs well.

Further, the Adaboost model displays significantly improved LOOCV performance for the majority of characteristics, yielding positive R^2 values for C, Pol, MR, ST, and MV. Notably, Adaboost exhibits significant robustness under the strict LOOCV methodology, with notably high prediction accuracy for Pol and P, along with low RMSE, MAE, and MAPE values. Furthermore, the comparatively low negative MPE values indicate that the Adaboost forecasts have no systematic bias. Negative

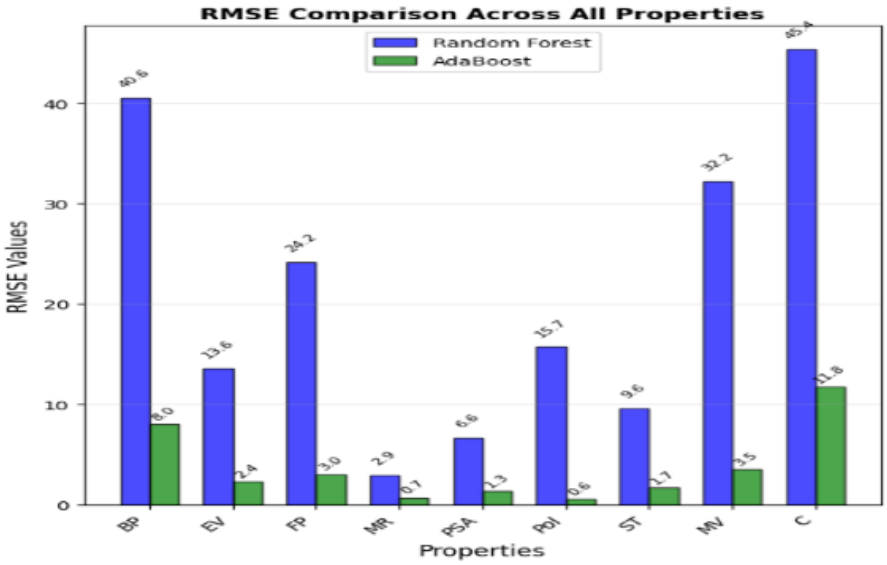

FIGURE 17. RMSE Matrices Comparison for Properties.

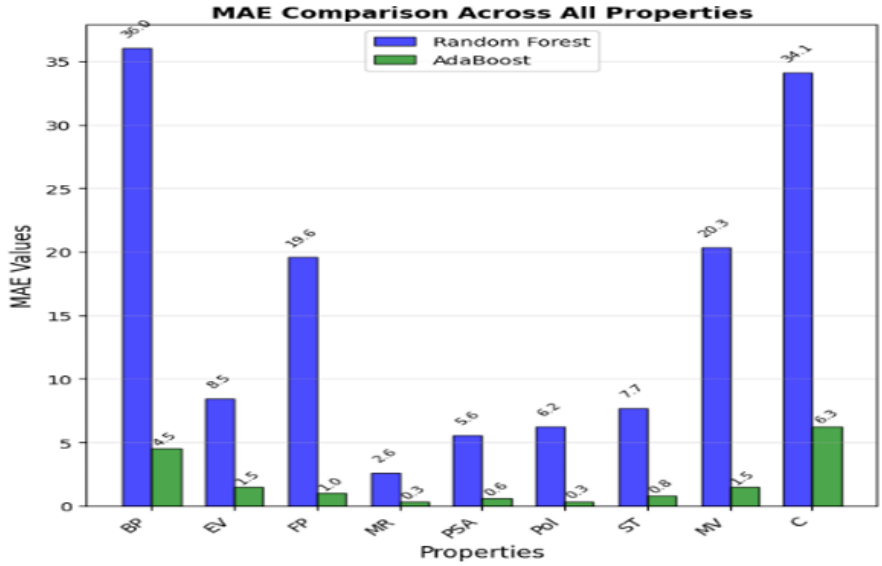

FIGURE 18. MAE Matrices Comparison for Properties.

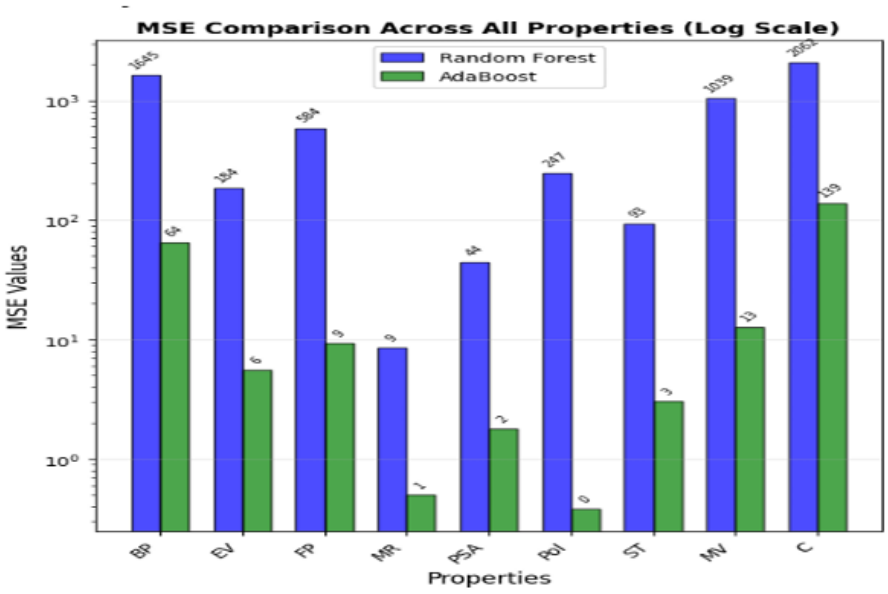

FIGURE 19. MSE Matrices Comparison for Properties.

R^2 values, on the other hand, suggest weak descriptor property correlations or inadequate model flexibility for MR and PSA, where degree six performs poorly.

Additionally, Adaboost produces lower absolute MPE and MAPE values, which represent improved prediction stability and less relative error. However, under LOOCV, Adaboost yields poor or negative R^2 values for BP, EV, FP and PSA underscoring the intrinsic challenge of modeling these attributes and the vulnerability of ensemble based techniques to small sample sizes in a leave-one-out context.

Overall, the LOOCV study shows that random forest and Adaboost can capture nonlinear structural property relationships. Whereas linear, quadratic and cubic regressions are inappropriate for the current dataset. With random forest acting as a potent complementary strategy, Adaboost was chosen as the main predictive model in this study because it provides the most consistent trade-off between predicted accuracy, error magnitude and percentage based performance indicators among the investigated models.

Table 13. LOOCV performance comparison of curvilinear models, RF and Adaboost.

Property	Model	RMSE	MAE	MPE (%)	MAPE (%)
BP	Linear Regression	357.518	262.731	-16.277	46.593
	Quadratic Regression	269.972	199.493	10.943	35.866
	Cubic Regression	282.302	241.796	22.329	43.093
	Bicubic Regression	23317.46	12805.91	-101.847	2272.911
	Random Forest	98.563	82.497	-0.594	14.775
	Adaboost	122.078	104.063	-0.287	18.347
EV	Linear Regression	45.069	33.394	-13.053	38.017
	Quadratic Regression	38.525	28.089	10.415	31.781
	Cubic Regression	45.195	29.971	19.755	34.691
	Bicubic Regression	2424.733	1347.799	-98.489	1493.394
	Random Forest	12.474	10.868	-0.075	12.258
	Adaboost	14.541	12.225	0.065	13.742
MR	Linear Regression	36.692	28.822	-1.415	39.067
	Quadratic Regression	21.478	17.033	0.339	19.237
	Cubic Regression	37.427	30.286	-14.362	37.686
	Bicubic Regression	2486.276	1403.671	-96.944	1487.847
	Random Forest	14.439	10.13	-13.2	19.306
	Adaboost	14.237	9.025	-14.667	18.173
PSA	Linear Regression	99.494	72.657	-40.25	91.912
	Quadratic Regression	35.62	22.25	-15.312	29.014
	Cubic Regression	69.125	37.751	-23.931	50.862
	Bicubic Regression	1523.403	809.834	-324.456	1074.396
	Random Forest	15.009	11.816	-2.685	14.134
	Adaboost	16.237	13.313	0.851	15.643
MV	Linear Regression	52	32.503	0.711	15.286
	Quadratic Regression	79.742	65.964	-16.195	33.918
	Cubic Regression	156.468	137.526	-38.887	66.447
	Bicubic Regression	12503.93	6981.773	-215.709	2462.64
	Random Forest	55.605	44.355	-18.707	31.505
	Adaboost	50.579	43.362	-16.306	28.651

Table 14. LOOCV performance comparison of curvilinear models, RF and Adaboost.

Property	Model	RMSE	MAE	MPE (%)	MAPE (%)
FP	Linear Regression	534.71	411.808	-50.428	144.686
	Quadratic Regression	514.335	344.578	22.668	117.999
	Cubic Regression	984.856	569.041	42.153	192.553
	Bicubic Regression	3545.919	2026.618	576.365	689.792
	Random Forest	63.663	45.058	0.695	16.062
	Adaboost	69.207	58.125	8.059	20.589
Pol	Linear Regression	14.652	11.507	-1.436	39.361
	Quadratic Regression	8.657	6.816	0.503	19.351
	Cubic Regression	14.968	12.113	-14.161	37.944
	Bicubic Regression	984.411	555.721	-95.843	1486.218
	Random Forest	5.671	3.928	-13.526	19.046
	Adaboost	5.806	3.763	-15.252	18.733
ST	Linear Regression	113.051	76.882	-91.106	145.986
	Quadratic Regression	85.388	67.977	40.076	119.301
	Cubic Regression	137.042	120.674	98.395	197.993
	Bicubic Regression	10252.48	5715.643	-1985.71	11640.69
	Random Forest	40.824	28.141	-7.011	36.625
	Adaboost	37.678	28.304	-4.704	37.964
C	Linear Regression	133.453	106.133	0.507	25.453
	Quadratic Regression	110.867	78.273	-7.217	16.913
	Cubic Regression	167.669	113.811	-14.889	25.773
	Bicubic Regression	9828.492	5578.069	69.699	922.327
	Random Forest	121.836	96.68	-10.996	23.27
	Adaboost	137.067	106.5	-11.98	24.704

8. Conclusion

This paper suggests a machine learning based approach for NEC based descriptors and computed QSPR analysis of commonly gout drugs. The analysis for linear, quadratic, cubic, random forest and Adaboost has done and compared graphically. The effectiveness of three regression techniques: linear regression, random forest and Adaboost to simulate increasingly complicated structure-property correlations was methodically evaluated. This restriction shows that linear models are unable to capture the nonlinear behavior typical of molecular descriptor property interactions, as evidenced by negative or low R^2 values, significant discrepancies between predicted and experimental values, and huge prediction errors.

The results depicts that Adaboost model vintages more precise and trustworthy outcomes. Moreover, the integration of molecular dynamics simulations, docking studies, and neighborhood eccentricity descriptors may return treasured insights into drug-target connections and facilitate the development of more selective compounds. This supports researchers in material science, environmental chemistry and drug development by enabling them to find novel medications and produce molecules with specific qualities. By taking these routes, investigators can meaningfully probe drug discovery improvements and create gout and other drugs in future. Moreover the intricate, non-linear relationships between these structural characteristics and the attributes that matter to us can be practically captured by machine learning. In the future, the emphasis should be on developing quicker algorithms for calculating descriptors, carefully choosing just the most pertinent features to prevent overcomplicating the model, and testing the method on a variety of chemical datasets to ensure that it truly functions in real world scenarios.

High R^2 values, lower RMSE, MAE, and good agreement in actual versus projected plots demonstrate Adaboost robust predictive performance for a number of characteristics, most notably MR and P. However, poorer results for IR and moderate prediction errors for FP, PSA, ST, and MV indicate that random forest partially captures the underlying nonlinearities and is still sensitive to descriptor selection and small data sets. Adaboost continuously shows better prediction accuracy and stability for the majority of physicochemical parameters among the assessed techniques. Higher order descriptor dependencies and intricate non-linear interactions are successfully modeled by its random forest and Adaboost framework, which is superior to linear, quadratic and cubic regression models. Strong agreement between experimental and anticipated values, low error metrics, and almost unity R^2 values all demonstrate this benefit.

LOOCV was used to further investigate the robustness of the model, offering a rigorous evaluation of generalization on the dataset. The variable generalization of random forest and Adaboost across characteristics and the instability of curvilinear regression are confirmed by the LOOCV analysis. Adaboost, on the other hand, consistently strikes a compromise between error magnitude, percentage based metrics, and predictive accuracy, which supports its use for physicochemical property prediction. Overall, the results highlight the need for ensemble based and nonlinear learning techniques in the modeling of complicated molecular systems. Within the suggested framework, Adaboost and random forest are robust models and even though curvilinear regression is straightforward. This study emphasizes the expanding use of sophisticated machine learning methods in QSPR modeling and drug discovery computation.

CREDIT AUTHORSHIP CONTRIBUTION'S STATEMENT

Nadeem Ul Hassan Awan carried out computational investigation, analysis, methodology and wrote the manuscript. Abdul Ghaffar worked on conceptualizations, figures, analysis and editing.

DECLARATIONS

Conflict of Interest: The authors declared that there is no conflict of interest regarding the publication of this research.
Funding: Authors received no funding for this research work.
Data Availability: The authors declare that the data supporting the findings of this study are available within the paper.

REFERENCES

[1] A. Ahmad, M. Farman, A. Ghafar, M. Inc, M. O. Ahmad and N. Sene, *Analysis and simulation of fractional order smoking epidemic model*, Computational and Mathematical Methods in Medicine **2022** (2022), 9683187.

[2] W. Ahmed, T. Ashraf, M. T. Saleem, E. E. Mahmoud, K. Ali, S. Zaman and M. B. Belay, *Computational approaches in drug chemistry leveraging python powered QSPR study of antimalaria compounds by using artificial neural networks*, Scientific Reports **15**, No.1 (2025), 19307.

[3] K. M. Asghari, M. Zahmatyar, F. Seyedi, A. Motamedi, M. Zolfi, S. J. Alamdary and S. Safiri, *Gout: global epidemiology, risk factors, comorbidities and complications: a narrative review*, BMC Musculoskeletal Disorders **25**, No.1 (2024), 1047.

[4] K. Balasubramanian, *Mathematical and computational techniques for drug discovery: promises and developments*, Current Topics in Medicinal Chemistry **18**, No.32 (2018), 2774-2799.

[5] K. T. Clebak, A. Morrison and J. R. Croad, *Gout: rapid evidence review*, American Family Physician **102**, No.9 (2020), 533-538.

[6] E. Estrada, L. Torres, L. Rodriguez and I. Gutman, *An atom-bond connectivity index: Modeling the enthalpy of formation of alkanes*, Indian Journal of Chemistry **37** (1998), 849-855.

[7] M. Ezekiel and K. A. Fox, *Methods of correlation and regression analysis: Linear and curvilinear*, (1959).

[8] M. Farman, A. Talib, K. S. Nisar, A. Sambas, M. Bayram and M. Hafez, *Investigation of ABPV predict dynamics infection in honeybee colony production: Soft patterns multiscale modeling with fractional approach*, Ain Shams Engineering Journal **16**, No.10 (2025), 103626.

[9] M. Farman, *Stability and chaos control of a fractional-order model for CO2 emissions in the environment*, Modeling Earth Systems and Environment **11**, No.4 (2025), 258.

[10] J. D. FitzGerald, N. Dalbeth, T. Mikuls, R. Brignardello-Petersen, G. Guyatt, A. M. Abeles and T. Neogi, *2020 American College of Rheumatology guideline for the management of gout*, Arthritis & Rheumatology **72**, No.6 (2020), 879-895.

[11] S. Fajtlowicz, *On Conjectures of Graffiti II*, Congressus Numerantium **60** (1987), 189-197.

[12] L. R. M. Gnanaraj, D. Ganesan and M. K. Siddiqui, *Topological indices and QSPR analysis of NSAID drugs*, Polycyclic Aromatic Compounds **43**, No.10 (2023), 9479-9495.

[13] I. Gutman, *On hyper-Zagreb index and coindex*, Bulletin (Académie serbe des sciences et des arts. Classe des sciences mathématiques et naturelles. Sciences Mathématiques) **42** (2017), 1-8.

[14] I. Gutman, *Geometric approach to degree-based topological indices: Sombor indices*, MATCH Communications in Mathematical and in Computer Chemistry **86** (2021), 11-16.

[15] S. Hayat, S. J. Alanazi and J. B. Liu, *Two novel temperature-based topological indices with strong potential to predict physicochemical properties of polycyclic aromatic hydrocarbons with applications to silicon carbide nanotubes*, Physica Scripta **99**, No.5 (2024), 055027.

[16] M. Imran, M. K. Siddiqui, S. Ahmad, M. F. Hanif, M. H. Muhammad and M. R. Farahani, *Topological properties of benzenoid, phenylenes and nanostar dendrimers*, Journal of Discrete Mathematical Sciences and Cryptography **22**, No.7 (2019), 1229-1248.

[17] S. Jamil, P. A. Naik, M. Farman, M. U. Saleem and A. H. Ganie, *Stability and complex dynamical analysis of COVID-19 epidemic model with non-singular kernel of Mittag-Leffler law*, Journal of Applied Mathematics and Computing **70**, No.4 (2024), 3441-3476.

[18] Y. Kara, Y. S. Özkan, A. Ullah, Y. S. Hamed and M. B. Belay, *QSPR modeling of some COVID-19 drugs using neighborhood eccentricity-based topological indices: A comparative analysis*, PLoS One **20**, No.5 (2025), e0321359.

[19] F. Khan, A. Zehra, M. Farman, K. S. Nisar, A. Sambas and M. Hafez, *Caputo gH-differentiability for Gronwall's inequality: insight, new results and application*, Journal of Inequalities and Applications **2025**, No.1 (2025), 148.

[20] S. A. K. Kirmani, P. Ali and F. Azam, *Topological indices and QSPR/QSAR analysis of some antiviral drugs being investigated for the treatment of COVID-19 patients*, International Journal of Quantum Chemistry **121**, No.9 (2021), e26594.

[21] A. N. Koam, M. Azeem, M. K. Jamil, A. Ahmad and K. H. Hakami, *Entropy measures of Y-junction based nanostructures*, Ain Shams Engineering Journal **14**, No.4 (2023), 101-123.

[22] V. R. Kulli, *Nirmala index*, International Journal of Mathematics Trends and Technology **67** (2021), 1045.

[23] V. R. Kulli, B. Chaluvaraju and T. V. Asha, *Computation of Nirmala indices of some chemical networks*, Journal of Ultra Scientist of Physical Sciences-A **33**, No.4 (2021), 30-41.

[24] T. R. Mikuls, Q. Soto, A. Petro, L. Helget, P. Roul, H. Sayles and B. R. England, *Comparison of rates of lower extremity amputation in patients with and without gout in the US Department of Veterans Affairs Health System*, JAMA Network Open **5**, No.1 (2022), e2142347-e2142347.

[25] B. Mohar, *Eigenvalues, diameter, and mean distance in graphs*, Graphs and Combinatorics **7**, No.1 (1991), 53-64.

[26] S. Nasir, F. B. Farooq, N. U. Hassan Awan and S. Parveen, *Topological indices of novel drugs used in blood cancer treatment and its QSPR modeling*, AIMS Mathematics **7**, No.7 (2022), 11829.

[27] S. Nasir, *Topological descriptors of colorectal cancer drugs and characterizing physical properties via QSPR analysis*, International Journal of Analytical Chemistry **2025**, No.1 (2025), 5512172.

[28] K. Pattabiraman, S. Sudharsan and M. Cancan, *QSPR modeling with topological indices of some potential drugs against cancer*, Polycyclic Aromatic Compounds **44**, No.2 (2024), 1181-1208.

[29] S. Parveen, N. U. Hassan Awan, F. B. Farooq and S. Hussain, *Topological Descriptors and QSPR Models of Drugs used in Blood Cancer*, Punjab Univ. J. Math. **55**, No.1 (2023), 27.

[30] L. Punzi, L. Scagnellato, P. Galozzi, C. Baggio, A. Damasco, F. Oliviero and R. Ramonda, *Gout: one year in review 2025*, Clinical and Experimental Rheumatology **43**, No.5 (2025), 799-808.

[31] M. Randic, *On characterization of molecular branching*, Journal of the American Chemical Society **97** (1975), 6609-6615.

[32] M. W. Rasheed, A. Mahboob and I. Hanif, *On QSAR modeling with novel degree-based indices and thermodynamics properties of eye infection therapeutics*, Frontiers in Chemistry **12** (2024), 1383206.

[33] A. Sabljić, *Topological indices and environmental chemistry*, Practical applications of quantitative structure-activity relationships (QSAR) in environmental chemistry and toxicology, 61-82, (1990).

[34] F. Saeed and N. Idrees, *Structural modeling of plant regulators based on topological indices and curve fitting*, Punjab Univ. J. Math. **57**, No.5 (2025), 576-590.

[35] F. Sivera, M. Andrés, L. Carmona, A. S. Kydd, J. Moi, R. Seth and D. M. Van Der Heijde, *Multinational evidence-based recommendations for the diagnosis and management of gout: integrating systematic literature review and expert opinion of a broad panel of rheumatologists in the 3e initiative*, Annals of the Rheumatic Diseases **73**, No.2 (2014), 328-335.

[36] M. Suresh, F. T. Tolasa and E. Bonyah, *QSPR/QSAR study of antiviral drugs modeled as multigraphs by using TIs and MLR method to treat COVID-19 disease*, Scientific Reports **14**, No.1 (2024), 1-14.

[37] C. Tamilarasi and F. S. Raj, *Multilinear-regression models developed by four novel degree-based topological indices in QSPR analysis*, Journal of Algebra and Statistics **13**, No.2 (2022), 3173-3181.

[38] D. Vukicevic and B. Furtula, *Topological index based on the ratios of geometrical and arithmetical means of end vertex degrees of edges*, Journal of Mathematical Chemistry **46** (2009), 1369-1376.

[39] J. Wei, M. F. Hanif, H. Mahmood, M. K. Siddiqui and M. Hussain, *QSPR analysis of diverse drugs using linear regression for predicting physical properties*, Polycyclic Aromatic Compounds **44**, No.7 (2024), 4850-4870.

[40] Y. Xin, L. Kong, Z. Liu, Y. Chen, Y. Li, H. Zhu and C. Wang, *Machine learning and deep learning methods for cybersecurity*, IEEE Access **6** (2018), 35365-35381.

[41] C. Yokose, N. McCormick, N. Lu, A. D. Joshi, G. Curhan and H. K. Choi, *Adherence to 2020 to 2025 dietary guidelines for Americans and the risk of new-onset female gout*, JAMA Internal Medicine **182**, No.3 (2022), 254-264.

[42] S. Zaman, H. S. A. Yaqoob, A. Ullah and M. Sheikh, *QSPR analysis of some novel drugs used in blood cancer treatment via degree based topological indices and regression models*, Polycyclic Aromatic Compounds **44**, No.4 (2024), 2458-2474.

[43] S. Zaman, W. Ahmed, M. K. Siddiqui, A. Mumtaz and Z. Kosar, *Role of eccentricity based topological descriptors to predict anti-HIV drugs attributes with supervised machine learning algorithms*, Computers in Biology and Medicine **190** (2025), 110101.

[44] X. Zhang, M. J. Saif, N. Idrees, S. Kanwal, S. Parveen and F. Saeed, *QSPR analysis of drugs for treatment of schizophrenia using topological indices*, ACS Omega **8**, No.44 (2023), 41417-41426.

[45] B. Zhou and N. Trinajstić, *On a novel connectivity index*, Journal of Mathematical Chemistry **46** (2009), 1252-1270.

[46] H. Zhou, A. Mahboob, M. W. Rasheed, A. Ovais, M. K. Siddiqui and I. Z. Cheema, *On QSPR analysis of molecular descriptor and thermodynamic features of narcotic drugs*, Polycyclic Aromatic Compounds **44**, No.5 (2024), 3079-3099.